CPFSK Demodulation Techniques

Kanchan Mishra

Electronics and Communication Department, IIT Guwahati

B-TECH Thesis

Under the supervision of

Prof. Anil Mahanta

Department of Electronics and Communication Engineering

Indian Institute of Technology, Guwahati

May, 2007

CERTIFICATE

It is certified that the work contained in the thesis entitled "CPFSK Demodulation Techniques", submitted by Kanchan Mishra with roll number 03010242, in the partial fulfillment for the degree of Bachelor of Technology has been carried out under my supervision and this work has not been submitted elsewhere for any other degree.

Date:

Prof. Anil Mahanta
Department of ECE
IIT Guwahati

ACKNOWLEDGEMENTS

I wish to express my gratitude to my guide and mentor Prof. Anil Mahanta for his persistent efforts, enthusiasm and encouragement during the project and for sharing his time and knowledge with me.

I am also thankful to all my friends and batch mates for their good company during my stay in IIT Guwahati.

I would like to thank and dedicate this thesis to my parents, for the unfailing emotional support they have provided me with, throughout the four years of engineering. And finally, I thank God Almighty, for whatever I have achieved in life is only through his help, and an expression of his will.

Kanchan Mishra,
Department of ECE,
I.I.T. Guwahati,
May 2007.

Contents

List of Figures

Chapter 2

Chapter 3

Chapter 4

List of Tables

Chapter 1
Introduction

1.1 Background

CPFSK is a non-linear modulation scheme [1]. Continuous phase frequency shift keying (CPFSK) is potentially an attractive modulation scheme for use on channels whose performance is limited by thermal noise**.** Continuous-phase frequency shift keying (CPFSK) refers to an FSK modulation scheme wherein the phase is constrained to be continuous during a symbol transition. Thus, it also has a memory. The constraint of continuous phase affects the signal in three important ways:1)Transient effects are lessened at the symbol transitions, thereby offering spectral bandwidth advantages [2]. As, CPFSK has merely slope discontinuities, and no step discontinuities, so its PSD $S(f) \sim 1/f^4$, thereby resulting in faster decay, and smaller bandwidth. 2) Memory, imposed upon the waveform by continuous phase transitions, improves performance by providing for the use of several symbols to make a decision rather than the more common approach of making independent symbol-by-symbol decisions. 3) Since, only phase is modulated, CPFSK has a constant envelope [3, 4]. This allows use of a cheap, power-efficient Class C amplifier. There is no interï modulation distortion in amplifier, and thus no spectrum splatter.

Besides, the constant envelope is appropriate for nonlinear channels, as it will experience fewer adverse effects than a non-constant envelope signal. Generally, though, we canôt carry as many bits/sec in a given bandwidth with CPFSK as we can with linear modulation (e.g., BPSK with square root raised cosine), because we use only one coordinate (phase) and ignore the other (radius). However, an added attraction of CPM is the rich variety of ways to detect it ï ranging from cheap and average BER performance, to expensive and optimum BER performance. CPFSK can be demodulated coherently, using schemes based on Viterbi Algorithm [5], to give optimum BER performance. At

the same time, there exist simple optimum and sub-optimum non-coherent demodulation schemes as well.

Because of the above-mentioned advantages, CPFSK schemes are the preferred modulation schemes in most of the wireless communication applications. Amplifier cost is roughly proportional to its power, and PAs dominate the cost of base stations. On the other hand, expensive and power-hungry detectors arenôt welcome in handsets either. So, detection trade-offs give some design freedom. Some of the international standards using CPFSK modulation scheme, have been tabulated in Table 1.

Table 1.1.International standards in communication, with CPFSK as the preferred modulation scheme [© Rappaport, T.]

Name of system	Frequency (MHz)	Channel width (kHz)	Bit rate (kb/s)	Modulation scheme	Access scheme
GSM	890-915 m-b	200	270.8	GMSK	TDMA, 8/16 ch/carrier
CT-2	890-915 m-b	100	72	Binary CPFSK	FDMA
DECT	890-915 m-b	1728	1152	GMSK	TDMA, 12/24 ch/carrier

Minimum-shift keying (MSK) is a special and simplest case of CPFSK, with modulation index h=0.5. Minimum shift keying (MSK) is a constant envelope, spectrally-efficient modulation scheme [6] which has long been used in digital mobile radio applications including the communications standards such as Digital European Cordless Telecommunications (DECT) and Global System for Mobile Communications (GSM) [7], [8], [9]. In addition to its spectral efficiency, MSK has a good error performance and self-synchronizing capability [10]. Its simplicity lies in the variety of schemes available for its demodulation. GMSK can be viewed as a derivative of MSK. In GMSK, the side-lobes are further reduced by passing the modulating NRZ data waveform through a pre-modulation Gaussian pulse-shaping filter. Base band Gaussian pulse shaping smoothes

the phase trajectory of the MSK signal, and hence stabilizes the instantaneous frequency variations over time. This has the effect of considerably reducing the side-lobe.

CPFSK modulation with +/-200 KHz as the frequency deviation is the preferred modulation scheme in the design of 2.4 GHz RF/IF up/down converter. 2-, 4- and 8- level CPFSK modulation scheme is also used in Broadband Wireless IP systems and Wireless IP point to point systems, utilizing the spectrum in both the licensed bands (700 MHz, 1.5GHz, 2.3GHz, 2.5GHz, 2.7-2.9GHz and 3.3-3.8GHz) and unlicensed bands (900MHz, 2.4GHz and 5.8GHz), and capable of delivering data speeds of upto 4Mbps. Moreover, MSK modulated millimeter wave sub-carrier are generated for radio over fiber applications [11]. Trellis-coded CPFSK is used for micro-cellular wireless applications [12]. Power-line communication (PLC) has an advantage that it can use existing facilities for communication, but it may not be suitable for wide-band signal transmission due to the nature of the power-line. Hence, adaptive CPFSK modulation scheme robust to harsh power-line channel condition finds application in PLC [13]. The modulation parameters are initialized and adjusted during the data transmission without interrupt by using line probing technique. CPFSK implementations are also suitable in many telemetry applications [14].

1.2 Literature Survey

The most extensive work on CPM and CPFSK signals was done by Aulin and Sundberg [15, 16, 17, 18]. Due to their attractive properties, CPFSK schemes, in particular GMSK became the preferred modulation scheme in most of the wireless application standards, as mentioned in previous section. Of late, their application in unconventional areas of Power-line communication and telemetry has also been explored [13, 14].

The optimum receiver for a CPFSK signal consists of a correlator followed by a ML sequence detector that searches the paths through the state trellis for the minimum Euclidean distance path. The Viterbi algorithm is an efficient method for performing this search. The maximum likelihood sequence receiver appears to have the best compromise between power and bandwidth efficiency. The reception scheme is based on the Viterbi

algorithm in the same manner introduced by Forney [11] for baseband digital transmission. In fact, Forney [12] also showed that the Viterbi algorithm could be used as a basis for a demodulator for MSK signals. MSK signals are CPFSK signals with a modulation rate of İ . The complexity of the decoding algorithm where we assume that the receiver makes a maximum-likelihood (ML) decision by means of the Viterbi algorithm is proportional to the number of states of the transmitter.

Thus, Forney [5] discussed the use of the Viterbi algorithm for detection of coherent CPFSK and, in particular, the modulation index 0.5 case studied by DeBuda was examined. This was followed by several attempts at finding an optimum CPFSK demodulation scheme on similar lines. On parallel lines, work was on for correlation filter based optimum coherent and non-coherent demodulation schemes. Pelchat *et al.* discussed the distance properties and, hence, high SNR performance of coherently detected CPFSK waveforms for two and three bit observation intervals [19]**.** In addition, this paper discussed optimum coherent demodulation with infinite observation interval. De Buda [20] discussed the performance of coherent CPFSK with a modulation index of 0.5 and given a self -synchronizing receiver structure for this case. Pelchat and Adams [21] discussed the minimum probability of bit error for non-coherent receiver for the three-bit observation interval and they have shown that the low SNR performance can be estimated by the average matched filter concept. The performance of coherent and non-coherent CPFSK with varying observation intervals has been investigated in [22]. It has been observed that for non-coherent demodulation, a modulation index of 0.715 and an observation interval of 5-bit periods gives the optimum performance.

However, CPFSK signal can also be retrieved via non-coherent demodulation techniques, which are appropriate for multi-path fading channels. In recent times, attention has been diverted to the analysis of non-coherent demodulation schemes for CPFSK [23]. Since, non-coherent FSK, and thus non-coherent CPFSK are more common in real-life applications, the need to analyze non-coherent demodulation schemes automatically follows. Also literatures suggest that as data rates increase, the performance of non-coherent schemes further improves. Hence, with data rates soaring higher and higher, the

possibility of non-coherent schemes taking the front seat is very high. Even at moderate data rates, as in telemetric operations, non-coherent demodulation schemes have been shown to have satisfactory BER at practical SNR s [24]. Recently, zero-crossing based CPFSK demodulators have also been studied, and investigated [25], for MSK schemes in particular, and have been found to have a performance in terms of BER, that is approximately 1.5 dB inferior to optimum Viterbi algorithm based MSK demodulation, theoretically, and approximately, 2.5 dB inferior in actual simulations. Practical realization may degrade the performance further, resulting in around 3-4 dB degradation. Though non-optimal, this class of methods is far simpler to implement than the optimal method of the coherent demodulation combined with the Viterbi algorithm, which has been proved by a comparison between their performance and complexity.

1.3 Aim of the Project

The aim of the project work is to implement and investigate various CPFSK demodulation techniques. We aim to generate CPFSK signals at various modulation indexes, and compare their spectral characteristics in terms of power spectral density, and band-width requirement. The next stage is to demodulate the CPFSK signals corrupted due to a noisy or fading channel. The class of CPFSK demodulation techniques can be broadly classified as Coherent demodulation techniques and Non-coherent demodulation techniques. Through the project, we wish to present a comparative study of various coherent and non-coherent demodulation schemes, their implementation complexity, and BER performance. The focus of our work is on exploring various non-coherent demodulation techniques. Based on the results obtained, we aim to be able to suggest possible applications of the non-coherent demodulation schemes discussed above.

1.4 Contributions

As a part of the project, we implemented the following algorithms in Matlab and tried dealing with some of the practical design issues, such as clock and carrier recovery and practical filter design issues for the same. The following algorithms were implemented to perform CPFSK modulation:

1. Trellis-based CPFSK modulation: The modulation is performed through the intermediate step of phase-tree construction. The phase-tree thus obtained is then used to obtain the CPFSK modulated signal.
2. FSM-based MSK modulation: The modulation is performed by constructing the state diagram and implementing thereof.

Since, spectral characteristics of CPFSK signals are their most attractive attribute, so the next step is to obtain the spectral characteristics of CPFSK signals thus obtained and compare their spectral characteristics to that of other contemporary modulation schemes. The next step is to perform demodulation of the CPFSK signals. The demodulation techniques implemented are broadly grouped as:

A. Coherent demodulation techniques: This class of demodulation techniques give optimal performance for CPFSK demodulation but at the cost of increased complexity. The following are some of the commonly used algorithms:

   A.1 Viterbi algorithm based MSK demodulation.

   A.2 Correlation receiver based coherent demodulation.

   A.3 Zero-crossing detector based coherent demodulation.

B. Non-coherent demodulation techniques

   B.1 <u>CPFSK as a special case of FSK:</u> Since, CPFSK is a special case of FSK, thus CPFSK can be demodulated using schemes used for simple FSK demodulation [26]. The following non-coherent FSK demodulation schemes were used for CPFSK demodulation:

   - FM detector-type FSK demodulator.
   - Demodulation using spectrally-matched filter and envelope detection.

   B.2 <u>Non-coherent CPFSK demodulation techniques:</u> This class of CPFSK demodulation techniques is although non-coherent, but in the decision block, they exploit the inherent memory characteristic of CPFSK signals and thus improve the performance [23]. We have the following two classes of decision mechanisms, to be discussed in next section.

   - Decision mechanism 1
   - Decision mechanism 2

The first stage in this scheme is non-coherent FM demodulation. Thus, the choice of FM demodulation scheme also has an impact on the performance and complexity.

B.3 Correlation filter based non-coherent CPFSK demodulation: This class of demodulation schemes gives the optimum performance among all schemes discussed so far. Their performance varies primarily by varying modulation index and data-rate. The accuracy of decision also increases as the observation interval is increased to some extent, and then starts degrading again [21,22].

B.4 Zero-crossing based demodulation: Finally, a zero-crossing based CPFSK demodulation scheme is investigated and simulated for an MSK signal. This scheme performs sub-optimally, but gives satisfactory performance in most practical cases [25].

1.5 Thesis organization

The rest of the thesis is organized as follows. Chapter 2 deals with the CPFSK modulation techniques used, viz. trellis-based modulation and state-machine based modulation. Section 2.3 deals with the spectral characteristics of CPFSK signals, and the effect of modulation index on it. Section 2.4 compares the spectral characteristics of CPFSK signals with other contemporary modulation schemes in order to explain why CPFSK has a cutting-edge over the rest.

In Chapter 3, the major coherent CPFSK demodulation schemes have been discussed. Section 3.1 describes the Viterbi algorithm based MSK demodulation, Section 3.2 describes the Correlation receiver based coherent demodulation and Section 3.3 discusses the Zero-crossing detector based coherent demodulation. The results and the discussion corresponding to each demodulation scheme are included as the respective subsections.

Chapter 4 describes the non-coherent CPFSK demodulation schemes implemented. The demodulation schemes developed assuming CPFSK as a special case of FSK, are described in Section 4.1. Sub-sections 4.1.1 and 4.1.2 discuss the sub-types of it, viz. FM

detector-type FSK demodulator and Matched-filter type FSK demodulator. The non-coherent CPFSK demodulation techniques which exploit the memory property of CPFSK are described in Section 4.2. Sub-section 4.2.1 describes the non-coherent FM demodulator block implementation of the demodulation mechanism described in Section 4.2. Sections 4.2.2 and 4.2.3 describe two possible implementations of the decision block of the scheme described in Section 4.2. Correlation filter based demodulation scheme is described and discussed in Section 4.3, while Section 4.4 discussed the Zero-crossing detector based non-coherent demodulator.

Finally, Chapter 5 summarizes the thesis and presents the possible future extensions.

Chapter 2
CPFSK Modulation

CPFSK modulation is similar to FSK modulation except that the condition of phase continuity is imposed at symbol transitions. This result in memory inherent in CPFSK signals in the form of phase information carried from previous symbol to current symbol. The modulation can be performed in several ways. The most basic method of generation of CPFSK signals is through construction of phase tree. Another method is through implementation of a state machine. These two modulation schemes have been discussed in Section 2.1 and 2.2, respectively.

Depending on the pre-modulating filter used (filtered data impulse) we consider the following classes of CPFSK modulated signals:

- integral response CPFSK modulated signals defined by modulating impulses extending over one symbol period:

$$g(t) = \begin{cases} \neq 0; t \in (0, T_s) \\ = 0; otherwise \end{cases}$$

- partial-response CPFSK modulated signals defined by modulating impulses extending over more symbol periods:

$$g(t) = \begin{cases} \neq 0; t \in (0, LT_s) \\ = 0; otherwise \end{cases}$$

The most frequently employed pre-modulating filters by the CPFSK modulations are LRC (Raised Cosine in time), LSCR (Raised Cosine in frequency) and LREC (Rectangular Impulse).

Spectral efficiency is the most attractive attribute of CPFSK signals. Thus, we analyze the spectral characteristics of the generated CPFSK signals in the subsequent sections.

2.1 Trellis-based CPFSK modulation

A carrier-modulated CPFSK signal s(t) can be expressed as (1):

$$s(t) = \sqrt{\frac{2E}{T}}\cos(2\pi f_c t + \phi(t;I) + \phi_0)$$

where, E represents the symbol energy, T is the symbol duration time, f_c is the carrier frequency and $\phi(t;I)$ is the information phase represented as:

$$\phi(t;I) = 2\pi f_d T \sum_{k=-\infty}^{n-1} I_k + 2\pi f_d (t-nT) I_k$$
$$= \theta_n + 2\pi h I_n q(t-nT)$$

Here, f_d is the peak frequency deviation, h is the modulation index such that, $h=2f_dT$, θ_n denotes the phase accumulation of the symbols up to time $(n-1)T$, i.e.,

$$\theta_n = \pi h \sum_{k=-\infty}^{n-1} I_k$$

And, $q(t)$ is the integral of the impulse response of the pre-modulating filter, and for a rectangular pre-modulating filter is defined as,

$$q(t) = \begin{cases} 0; t<0 \\ t/2T; 0 < t < T \\ 1/2; t>T \end{cases}$$

where, T corresponds to a bit period.

2.1.1 Results and Discussions

The following figure 2.1(b) illustrates the construction of phase tree based on the information in section 2.1, corresponding to the NRZ data-stream shown in figure 2.1(a). Figure 2.2 shows the input base-band NRZ signal and the corresponding CPFSK signal constructed using the process of phase tree construction as in the figure above. The phase information obtained by phase tree construction gives $\phi(t;I)$ given in equation (2.4) which is then integrated in equation (2.3) to obtain the CPFSK signal s(t).

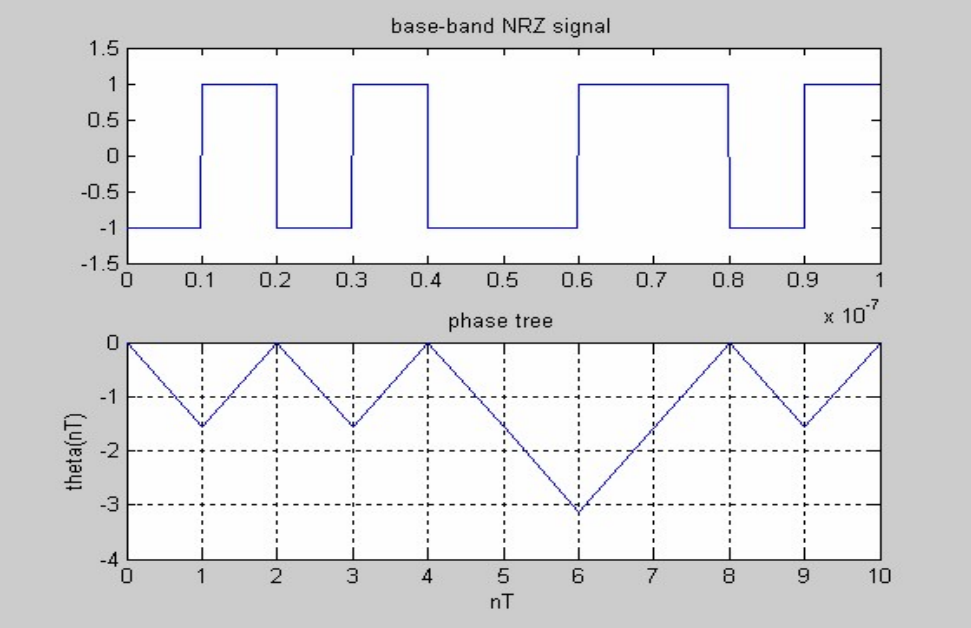

Figure 2.1: (a) Input NRZ data-stream, (b) corresponding phase-tree. (N=10)

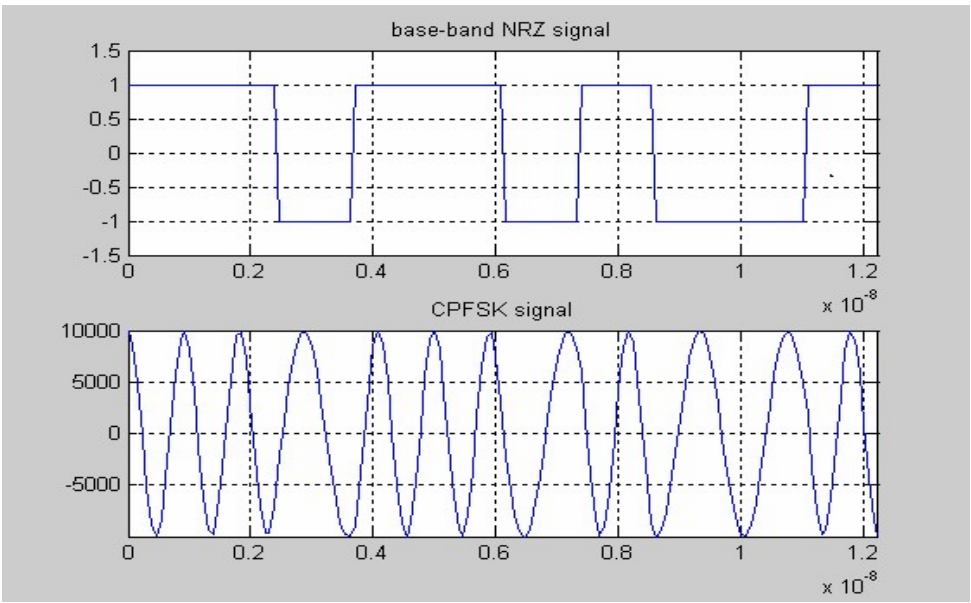

Figure 2.2: (a) Input NRZ data-stream, (b) corresponding CPFSK signal. (N=10, h=0.5, fc= 900MHz, fd=200MHz, fs=13GHz)

2.2 FSM-based CPFSK modulation

In FSK, a digital input sequence ***u*** selects one of ***m*** frequencies (if u_k is m-ary) in each signaling interval of length T; that is, the transmitted signal $\eta(t)$ is

$$\eta(t) = \cos[\omega(u_k)t + \theta_k], kT \le t \le (k+1)T$$

where, ϒ(u_k) is the frequency selected by u_k , and ϑ$_k$ is some phase angle. It is desirable for reasons both of spectral shaping and of modulator simplicity that the phase be continuous at the transition interval; that is, that

$$\omega(u_{k-1})kT + \theta_{k-1} \equiv \omega(u_k)kT + \theta_k \bmod 2\pi$$

This is called continuous-phase FSK. The continuity of the phase introduces memory into the modulation process; i.e., it makes the signal actually transmitted in the k^{th} interval dependent on previous signals.

To take the simplest possible case (deviation ratio =1/2, i.e. modulation index =1/2), let the input sequence u be binary and let ϒ(0) and ϒ(1) be chosen so that ϒ(0) goes through an integer number of cycles in T seconds and ϒ(1) through an odd half-integer number; i.e. ϒ(0)T ∫ 0 and ϒ(1)T ∫ ´ modulo 2´. Then if ϑ$_0$=0, ϑ$_1$= 0 or ´, according to whether u_0 equals zero or one, and similarly ϑ$_k$= 0 or ´, according to whether an even or odd number of ones have been transmitted.

Here we have a two-state process, with X={0, ´}. The transmitted signal y_k is a function of both the current input u_k and the state x_k:

$$y_k = \cos[\omega(u_k)t + x_k] = \cos x_k \cos\omega(u_k)t, kT \le t < (k+1)T$$

Since transitions ζ$_k$ = (x_{k+1}, x_k) are one-to-one functions of the current state x_k and input u_k, we may alternately regard y_k as being determined by ζ$_k$. If we take η$_0$(t)= cos ϒ(0)t and η$_1$(t)= cos ϒ(1)t as bases of the signal space, we may write

$$y_k = y_{0k}\eta_0(t) + y_{1k}\eta_1(t)$$

where the coordinates y_{0k} and y_{1k} are given by

$$(y_{0k}, y_{1k}) = \begin{cases} (1,0), & \text{if } u_k = 0, x_k = 0 \\ (-1,0), & \text{if } u_k = 0, x_k = \pi \\ (0,1), & \text{if } u_k = 1, x_k = 0 \\ (0,-1), & \text{if } u_k = 1, x_k = \pi \end{cases}$$

Thus, the state machine of MSK generation is described by the following diagram and tables.

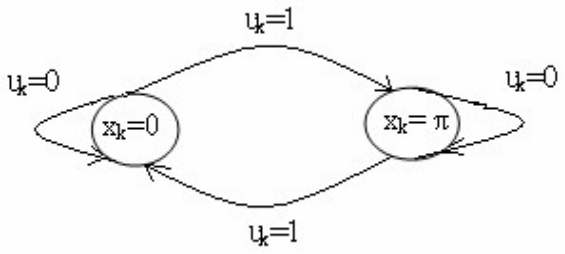

Figure 2.3: MSK State transition diagram

x_{k+1}

x_k / u_k	**0**	**p**
0	0	´
1	´	0

y_{0k}

x_k / u_k	**0**	**p**
0	1	-1
1	0	0

y_{1k}

x_k / u_k	**0**	**p**
0	0	0
1	1	-1

Table 2.1: (a) State transition table (b) output y_{0k} table (c) output y_{1k} table

2.3 Spectral Characteristics of CPFSK signal

The available channel bandwidth is limited in many digital communication systems. Consequently, the system designer has to consider the constraints imposed by the channel bandwidth limitations in selecting the modulation technique used to transmit the information. Thus, it is important to know the spectral content of digitally modulated signals. The spectral distribution is very important in furnishing bandwidth requirements and in evaluating mutual interference between neighboring channels. Also, power spectral density (PSD) is critically important in optimizing procedures. In many applications it is essential to know the frequencies and the extent to which sharp spectral peaks occur. These peaks can, under certain conditions, become delta functions causing severe crosstalk. Thus, estimation of Power Spectral Density (PSD) of a signal is one of the frequently used post-processing operations. This necessitated the need for PSD

computation of CPFSK signals. Figure 2.4 illustrates the obtained PSD of a CPFSK signal simulation.

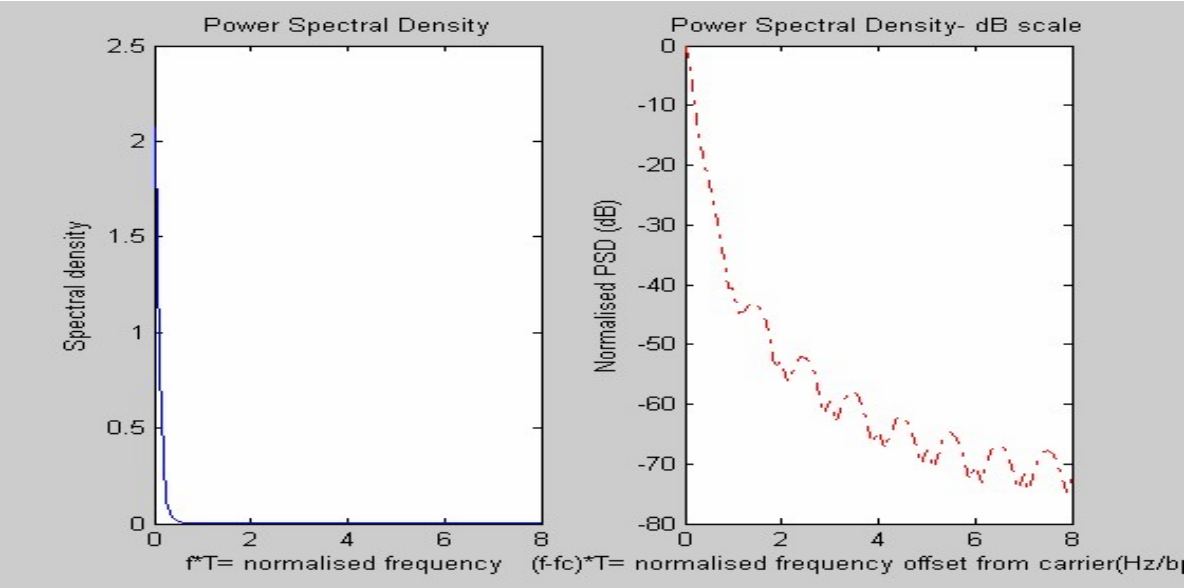

Figure 2.4: Power Spectral Density of a CPFSK signal (a) Linear scale, (b) dB scale. fs= 9600 Hz, fc=2400 Hz, fd=30 Hz, T=32 samples, R=300 bps, h=0.2, N=10000.

CPFSK signals are known to be the most spectrally efficient modulation scheme when compared to other contemporary modulation schemes. This is evident in Figure 2.5, that compares the power-spectral density of MSK (CPFSK with modulation index h=1/2), GMSK (Gaussian MSK- MSK with Gaussian pre-modulating filter) and QPSK signals.

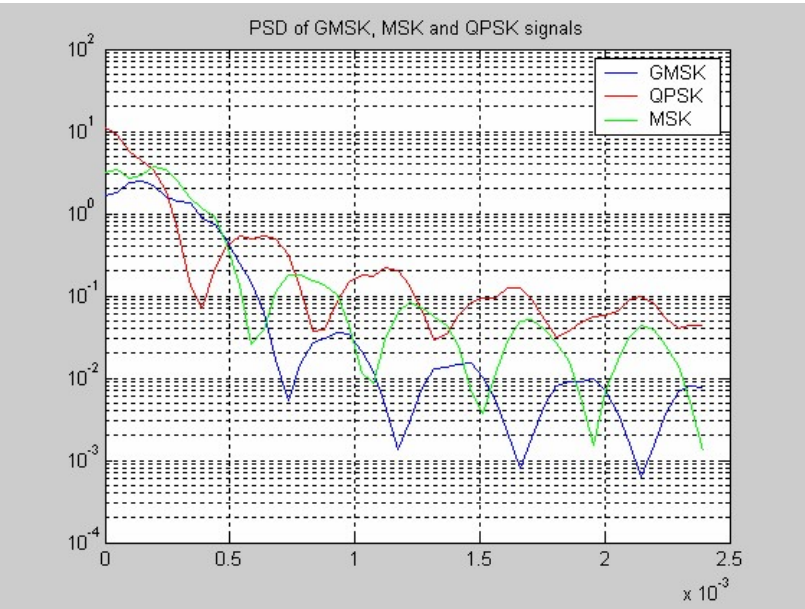

Figure 2.5: PSD comparison of GMSK, MSK and QPSK.

As can be seen from the figure, the main lobe width of MSK/ GMSK is approximately 1.5 times wider than QPSK. However, the side-lobes are lower for MSK and GMSK and roll-off faster. This results in MSK and GMSK having a smaller effective band-width, as compared to QPSK.

Another interesting feature can be observed from Figure 2.6, which compares the spectral characteristics of CPFSK modulated signals with respect to modulation index. It can be observed the band-width of a CPFSK signal increases with the modulation index. Besides, CPFSK signal is band-limited as long as the modulation index is in the interval (0, 1). When a modulation index greater than one is employed, the linear scale power-spectral density ceases to be band-limited. As will be seen in the subsequent chapters, several demodulation schemes give a BER performance that improves with increase in modulation index. This presents an important design trade-off between band-width requirement and BER performance.

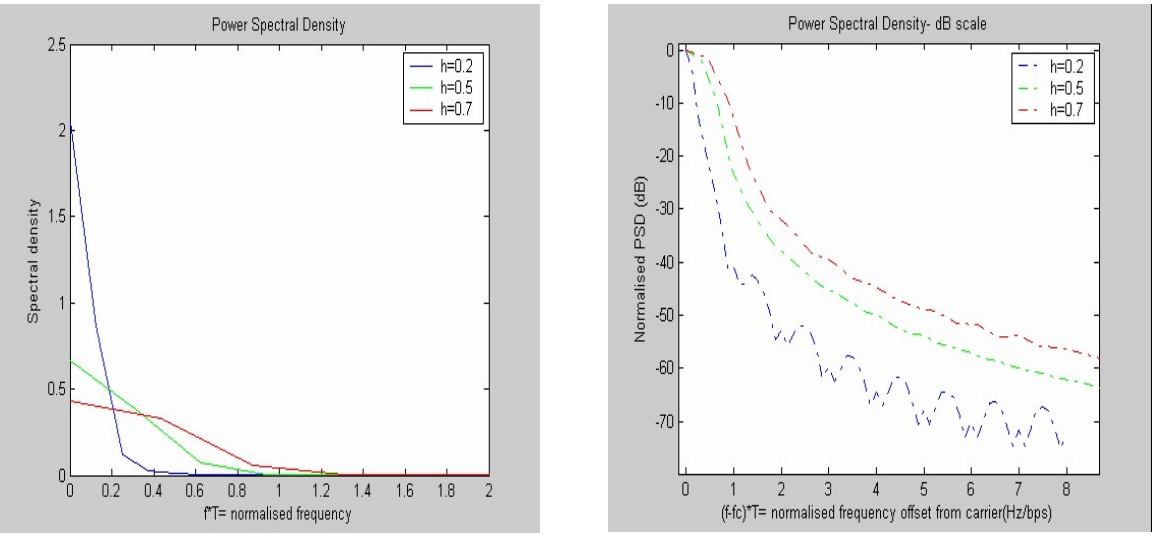

Figure 2.6: PSD comparison of CPFSK signals with modulation index (a) Linear scale (b) dB scale

2.4 Conclusions

Having generated a CPFSK signal and studied its spectral properties, the next step in a CPFSK system is its successful demodulation. This can be achieved in several ways, which are broadly categorized as ï coherent and non-coherent demodulation schemes, to be discussed in subsequent chapters.

Chapter 3

Coherent Demodulation Techniques for CPFSK

Coherent demodulation techniques are those requiring phase information of the carrier. These demodulation schemes require the local oscillator at the receiver to extract the phase information of the carrier signals used at the transmitter side, from the received signal, in order to generate coherent reference carrier signals. This increases the complexity involved in implementing a coherent receiver, but at the same time secures a better BER performance.

3.1 Viterbi Algorithm based Coherent demodulation of MSK

Referring to Section 2.2, where we discussed FSM based MSK modulation, if the received signal $z(t)$ is $\eta(t)$ plus white Gaussian noise $\nu(t)$, then by correlating the received signal against both $q_0(t)$ and $q_1(t)$ in each signal interval (coherent detection), we may arrive without loss of information at a discrete-time output signal

$$z_k = (z_{0k}, z_{1k}) = (y_{0k}, y_{1k}) + (n_{0k}, n_{1k})$$

where, n_0 and n_1 are independent equal-variance white Gaussian noise sequences. This model appears in Figure 3.1, where the signal generator generates (y_{0k}, y_{1k}) according to the aforementioned rules.

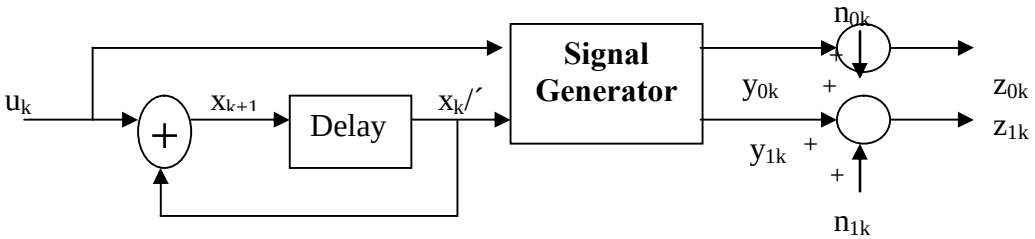

Figure 3.1: Model for binary MSK and coherent detection in white Gaussian noise.

The two-state trellis for MSK is shown in the figure 3.2 below. The Viterbi algorithm based demodulation of M-ary MSK involves moving through the trellis, and at the end of each bit period, retaining only the most likely path and discarding the rest, based on the correlator outputs.

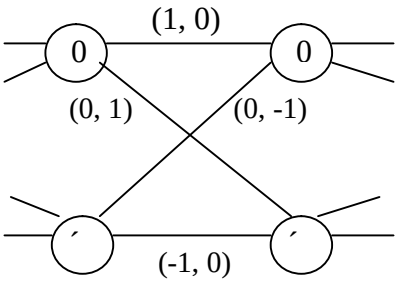

Figure 3.2: Phase- trellis for MSK

3.1.1 Results and Discussions

We know that the best probability of error one can do with coherent detection of orthogonal signals like FSK is given by:

$$P_e = Q\left(\sqrt{\frac{E_b}{N_0}}\right)$$

However, G.D. Forney showed in [5] that for MSK case, exploiting the memory doubles the effective signal energy, or improves the signal-to-noise ratio by 3dB, and the probability of error is given by:

$$P_e = Q\left(\sqrt{\frac{2E_b}{N_0}}\right)$$

Thus, as can be seen in Figure 3.3, CPFSK with a modulation index of İ , i.e. MSK is inherently 3 dB better than non-continuous phase FSK or as good as antipodal phase-shift keying.

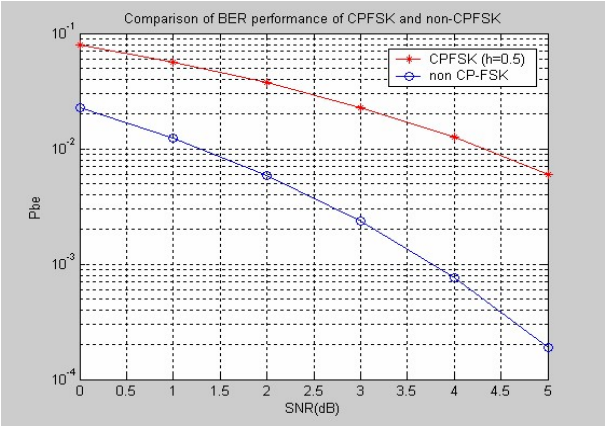

Figure 3.3: Comparison of BER performance for binary CPFSK (h=0.5) and non CP-FSK with coherent detection in white Gaussian noise.
(fs=9600 Hz, fc=2400 Hz, fd=30 Hz, T=32 samples, R=300bps, h=0.2, N=10000.)

3.2 Correlation filter based Coherent demodulation of CPFSK

In coherent correlation filter based demodulation of CPFSK, we define the coherent carriers corresponding to symbol 1 and symbol -1 sent, as below:

$$s_1(t,1) = \cos\left(\frac{\pi ht}{T}\right)\cos(2\pi f_c t)$$

$$s_2(t,1) = \cos\left(\frac{\pi ht}{T}\right)\sin(2\pi f_c t)$$

$$s_1(t,-1) = \sin\left(\frac{\pi ht}{T}\right)\cos(2\pi f_c t)$$

$$s_2(t,-1) = \sin\left(\frac{\pi ht}{T}\right)\sin(2\pi f_c t)$$

The block diagram of optimum coherent receiver as given in [24] is shown in Figure 3.4. The final decision is taken using Maximum-likelihood criterion.

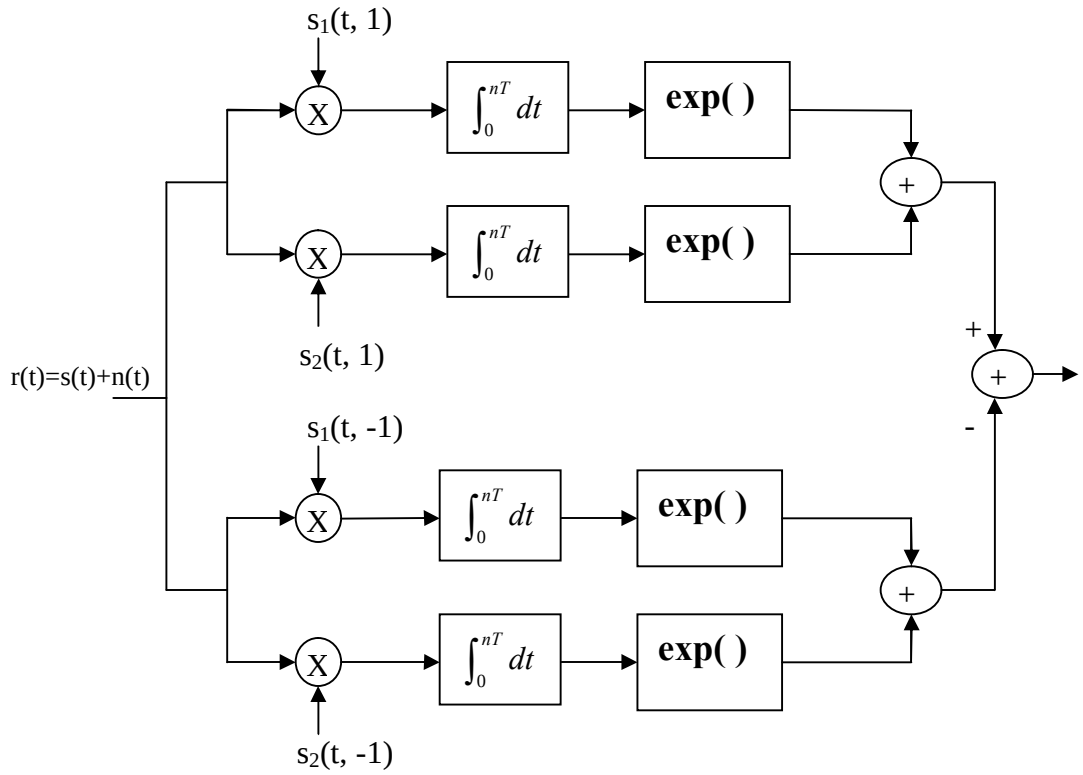

Figure 3.4: Block diagram of optimum coherent receiver

Decision is based on the sign of the computed metric l i.e., if l is positive, a decision is taken in favor of symbol 1, otherwise a decision is taken in favor of -1. The performance obtained with this type of receiver is similar to the performance obtained with 1 observation interval for MSK in Section 3.1.1.

3.3 ZCD based Coherent demodulation of CPFSK

Even though the Viterbi algorithm discussed in Section 3.1 is simple for a two-state trellis, literatures suggest that the complexity increases significantly as the number of states increase. Simpler sub-optimum coherent demodulation schemes can achieve effectively the same performance. An example of this was shown using the correlation filter based receiver of Section 3.2. We now discuss a much simpler scheme for coherent demodulation of CPFSK using the zero-crossing detector.

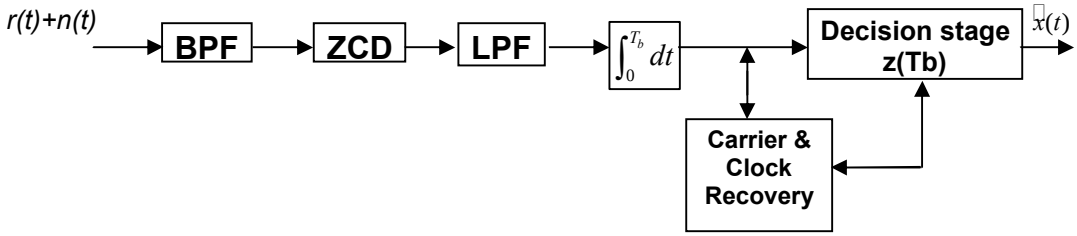

Figure 3.5: ZCD based coherent demodulator

The block diagram of the zero-crossing based coherent MSK demodulator is shown in Figure 3.5. The system is basically made up of a phase detector followed by a carrier and clock recovery and decision stages. The received signal $r(t) + n(t)$, after noise limiting, is fed to a zero-crossing detector (ZCD) which generates a sequence of positive impulses at its output.

The resultant signal is then low-pass filtered and integrated over a bit period to produce an output proportional to the instantaneous signal phase. Theoretically, samples of the accumulated signal phase at each zero crossing could have been obtained by directly integrating the ZCD output. However, this would enable one to know the phase values only where the zero crossings occur. As will be explained below, mid-bit and end-bit instantaneous phase values are needed for clock and carrier recovery. A low-pass filter (LPF) cascaded with the ZCD will provide the phase value at any instant over the bit

period. The end-bit sample is used for the decision and the mid-bit value, together with the end-bit value, by the clock and carrier recovery stage.

3.3.1 Carrier and Clock Recovery

The carrier recovery stage uses the mid-bit phase measurements from the signal to extract the phase reference. If the phase is rising, relative to the carrier phase during the bit period, then the mid-bit phase difference should be 45 degree more than the one at the start of the bit period. Similarly, if the phase is falling with respect to the carrier phase then the mid-bit phase difference should be 45 degree less than its value at the start of the bit period. By comparing the mid-bit phase with the expected one, the size and direction of the carrier error is obtained and a proportion of this error is used to correct the phase reference.

On the other hand, clock recovery is achieved by using a peak search algorithm. It uses three phase samples: two mid-bit samples from two consecutive bits and an end-bit sample between them. Considering the possibility that the phase trajectory relative to the carrier phase has a local maximum (or minimum) at the end of a bit period (this happens whenever a change in the received binary symbol occurs), the algorithm compares the differences in phase between three samples to determine the timing error.

3.3.2 Implementation Issues

The band-pass filter shown in the block diagram of ZCD based CPFSK demodulator is implemented using an FIR filter in order to have a linear phase response of the filter to maintain the phase continuity property of CP FSK signal. Its only aim is to band-limit the noisy received signal.

In order to realize a ZCD, one would hard-limit the input waveform, differentiate to accentuate the zero-crossing points and pass through a full-wave rectifier to eliminate negative pulses due to negative-going zero crossings as shown in Figure 3.6.

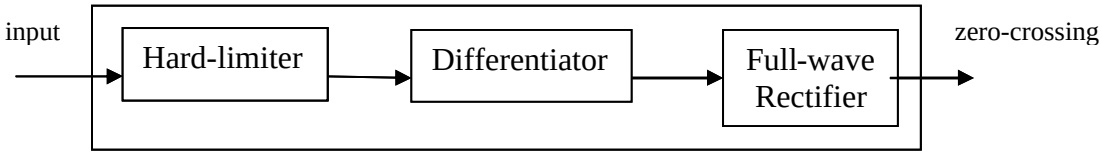

Figure 3.6: Realization of a Zero-Crossing Detector.

The output of the ZCD is fed to a LPF, the purpose of which is to interpolate the zero-crossings. Since, linear phase response of the filter is not a requirement in this case an IIR filter of suitable order and cut-off would suffice the requirement. In our design we used the butter-worth IIR filter design. The order of the filter and the cut-off parameters for the filter design depend on the system specifications such as carrier frequency, sampling frequency, deviation frequency and the desired attenuation in each of the bands.

The output of the integrator corresponding to a bit stream has been shown below. Decision as well as carrier and clock recovery use this output according to the aforementioned rules.

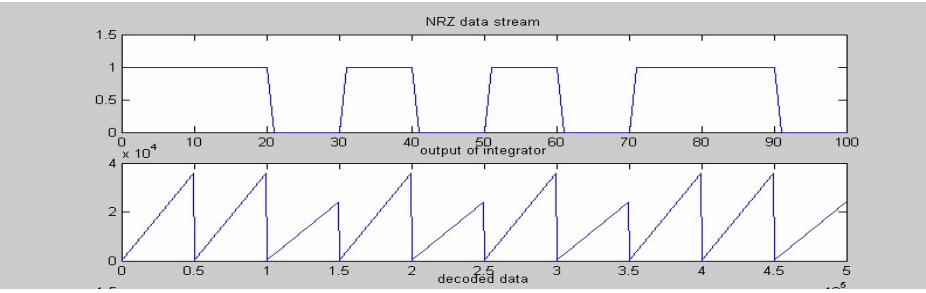

Figure 3.7: Input bit stream and corresponding integrator output

3.3.3 Results and Discussions

The BER performance obtained with this class of demodulators is sub-optimal as compared to that of demodulators explained in section 3.1 and 3.2. However, given the reduced complexity in carrier and clock recovery, as explained in section 3.3.1, the scheme turns out to be a feasible choice. The BER performance obtained with this type of demodulators is shown in the figure below.

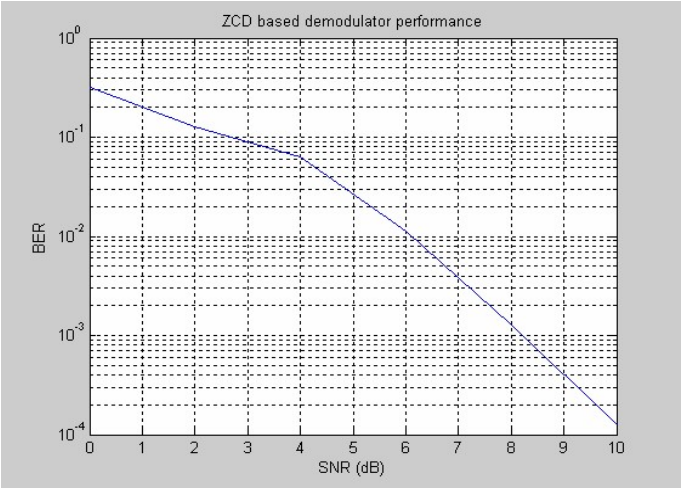

Figure 3.8: BER performance of ZCD based coherent CPFSK demodulator
fs=9600 Hz, fc=2400 Hz, T=32 samples, R=300bps, h=0.2, N=10000.

3.4 Conclusions

Coherent schemes for CPFSK demodulation give optimal to sub-optimal performance at a high to a moderate implementation complexity. However, there could be even simpler demodulation schemes for CPFSK demodulation with a fairly acceptable BER performance. This leads us to the next chapter where we explore the non-coherent CPFSK demodulation schemes.

Chapter 4
Non-Coherent Demodulation Techniques for CPFSK

Non-coherent continuous-phase FSK demodulation differs from coherent demodulation in that it does not require the phase information of the carrier signals used on the transmitter side to generate the reference carriers at the local oscillator on the receiver side. Thus, in a non-coherent receiver, the reference carriers at receiver might have a different phase than those at the transmitter and it may still be possible to secure the correct demodulation. As can be expected intuitively, the error performance slightly degrades for the non-coherent receiver. This is however, achieved at a complexity much less than that involved in a coherent receiver in the extraction of phase information.

4.1 CPFSK as a special case of FSK

This class of demodulators considers CPFSK as a special case of FSK. Thus, CPFSK can be demodulated using schemes used for simple FSK demodulation [26]. These modulation schemes do not exploit the inherent memory in CPFSK signals. The optimum error performance obtained theoretically, with this class of demodulators is given by,

$$P_e = \frac{1}{2}\exp\left(-\frac{E_b}{2N_0}\right)$$

In practice however, the performance is severely limited by implementation issues involved. The following non-coherent FSK demodulation schemes were implemented for CPFSK demodulation, as a part of this project.

4.1.1 FM detector-type FSK demodulator

The FM detector demodulator treats the FSK signal as a simple FM signal with binary modulation. Figure 2 shows a functional block diagram for an FM detector-type demodulator. The received FSK signal is band-pass filtered to remove out-of-band interference and then limited to remove AM interference. The limited signal is FM-detected to produce a positive output for a mark condition and a negative output for a space condition. The raw, detected signal is low pass-filtered to remove noise

components at frequencies above the baud rate, and, finally, the decision circuit makes all positive voltages into binary 1ôs and all negative voltages into binary 0ôs.

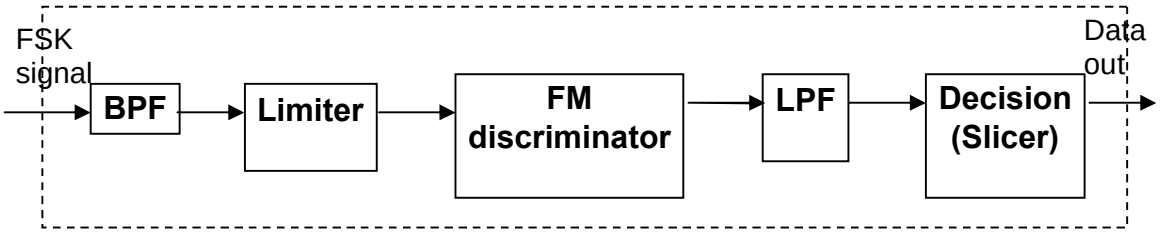

Figure 4.1: FM detector-type FSK demodulator

This type of demodulator was very popular due to its relative simplicity and its non-critical tuning. Phase-locked-loop (PLL) demodulators are a more recent technique, but they have very similar performances to that of FM detector demodulators. FM-type detectors are non-optimal in the sense that they perform more poorly than signal detection theory would predict is possible. The performance of an FM-type FSK detector is severely limited by its relatively wide input bandwidth. The inclusion of large portions of frequency spectrum that do not contain significant signal energy is clearly a non-optimal approach to FSK demodulation.

4.1.1.1 Implementation Issues

The band-pass filter shown in the block diagram of ZCD based CPFSK demodulator is implemented using an FIR filter in order to have a linear phase response of the filter to maintain the phase continuity property of CPFSK signal. Its only aim is to band-limit the noisy received signal.

The limiter shown in the block diagram is implemented as a hard-limiter followed by a band-pass filter centered on the carrier frequency to select the sinusoidal component at the frequency. The FM discriminator is implemented as a differentiator or a high-pass filter. A butter-worth IIR filter is used to design the high pass filter because IIR filters can obtain better transition band characteristics. The low pass-filtering is done to remove noise components at frequencies above the baud rate. Since, linear phase is not a

requirement at this stage; we implement this filter using a butter-worth IIR low-pass filter of suitable order and cut-off, depending on the system specifications.

4.1.1.2 Results and Discussions

As mentioned above, the performance of an FM detector-type FSK demodulator is severely limited by its relatively wide input bandwidth. The inclusion of large portions of frequency spectrum that do not contain significant signal energy is clearly a non-optimal approach to FSK demodulation. Their performance is quite poor, and in general, canôt be used for most practical applications, except for some dummy applications and demonstration purposes. Appropriate filter design is an important issue in this class of demodulators.

4.1.2 Matched-filter type FSK demodulator

Filter-type demodulators attempt to optimally match the FSK signal parameters to the demodulator configuration to optimize demodulator error performance. A simplified spectrum for filter-type demodulators is shown in Figure 4.2. The proper filter design depends not only on the signal parameters, but also on the nature of the signal interference. The classic ñmatchedò filter demodulator is optimal for coherent FSK in white Gaussian noise interference [26].

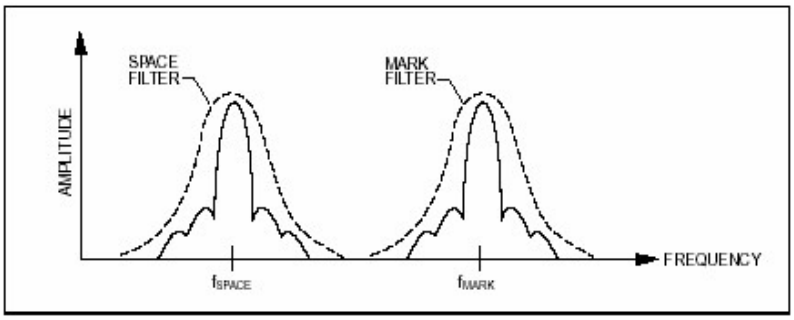

Figure 4.2: Simplified demodulation spectrum for matched-filter FSK demodulator

A block diagram of a simple, matched-filter demodulator for coherent FSK is shown in Figure 4.3. In the demodulator, the output of the matched filters is compared, and if the output from the mark filter is larger than that from the space filter, a decision is made that a mark signal was transmitted. Space detection is similarly performed.

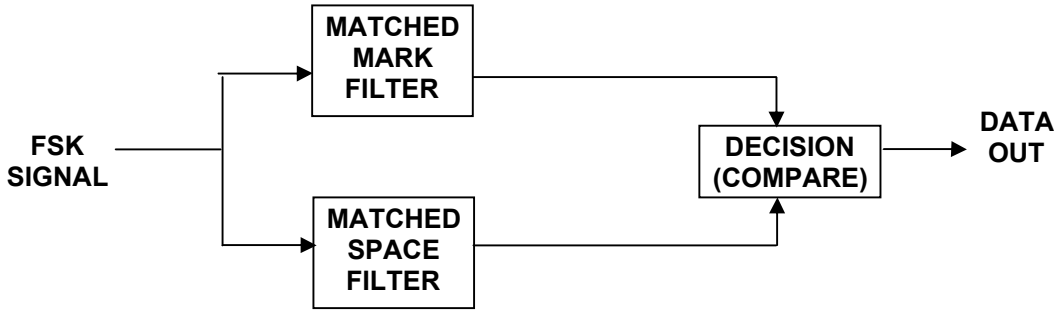

Figure 4.3: Coherent Matched-filter FSK demodulator.

Because non-coherent FSK is so much more common than coherent FSK, it is necessary to have a type of demodulator that does not depend on phase information. Optimum demodulation of non-coherent FSK can be achieved by envelope detection of the signal filter outputs in a filter-type demodulator. A demodulator of this type is shown in Figure 4.4. The outputs of the mark and space filters are envelope-detected and sampled at every t=kTb, where k is an integer, and their values compared to determine which has greater magnitude. Note that phase information is not required. With the ñrightò filter shape, performance of this type of demodulator approaches the theoretical optimum for non-coherent FSK. The ñrightò filter shape for a white noise interference environment is one that has the same spectral shape as the transmitted signal. However, inability to obtaining the right filter shape is what limits the performance in most practical scenarios as will be discussed in the next section.

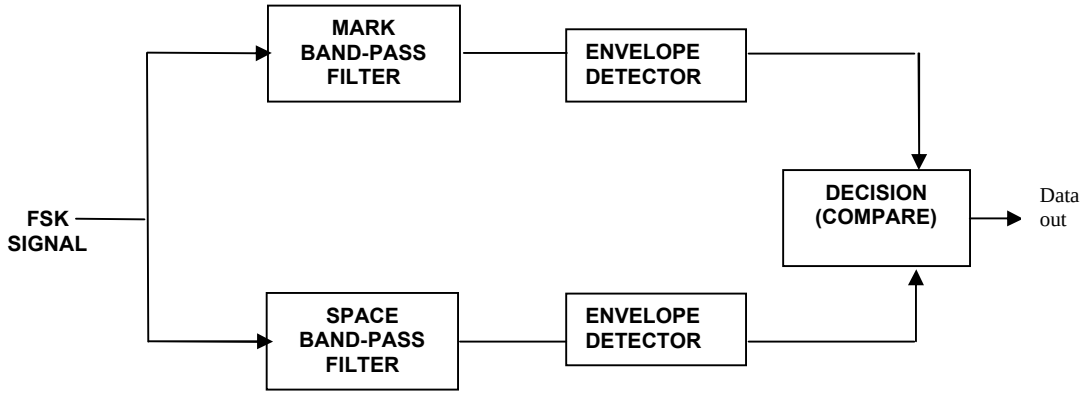

Figure 4.4: Non-coherent FSK demodulation with spectrally matched filters and envelope detection.

4.1.2.1 Implementation Issues

With the ñrightò filter shape, performance of this type of demodulator approaches the theoretical optimum for non coherent FSK. The ñrightò filter shape for a white noise

interference environment is one that has the same spectral shape as the transmitted signal. For the ñrectangularò modulation of FSK, the right shape is a sinc function band pass filter centered about the desired mark or space tone. The spectral shape of optimum mark and space filters is as shown in Figure 4.5.

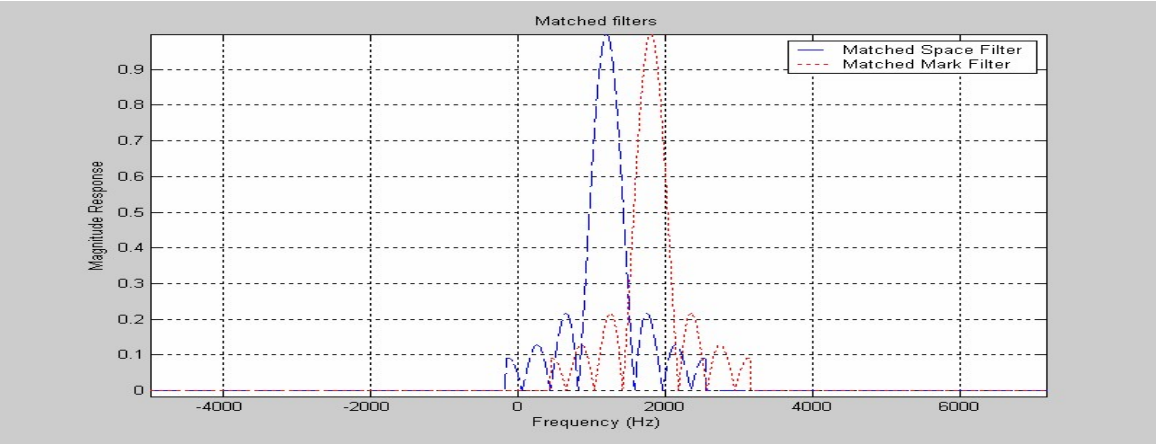

Figure 4.5: Matched Mark and Space filters
(fc=1500 Hz, fd=600 Hz, h=0.5, fs=27 kHz, R=2400bps, N=10000)

The ñrightò filter design is an important issue in Matched- filter type FSK demodulator. In practice, matched filter implementation of a non-coherent demodulation scheme seldom gives the optimum performance because of our inability to design the ideal spectrally matched filter.

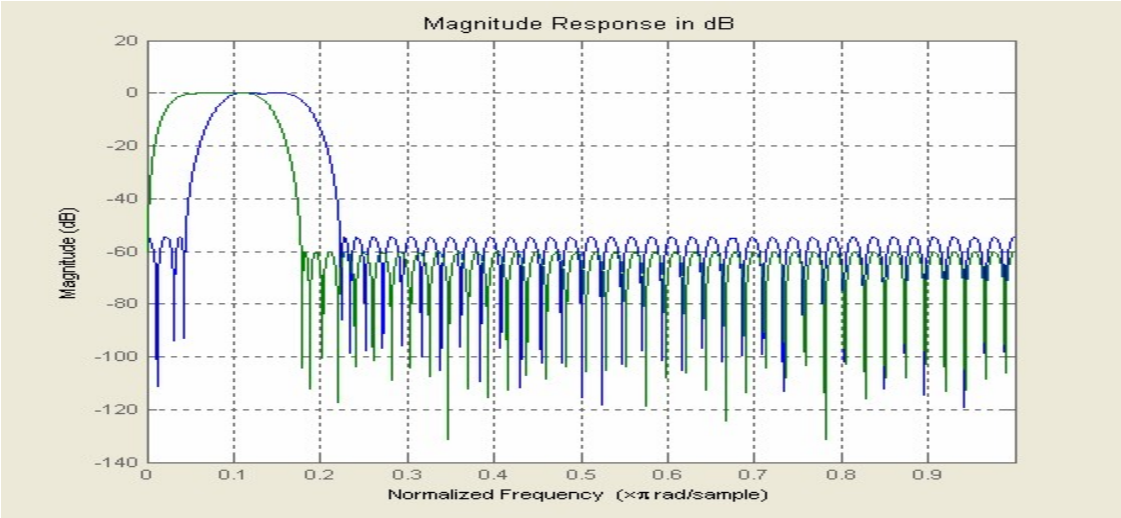

Figure 4.6: Frequency response of matched filters obtained using equiripple FIR filter design
Blue: Mark filter response, Green: Space filter response
Order: 86; fs=27 kHz, Dstop1=0.001, Dpass1=0.1, Dstop2=0.001
Mark filter: fmark: 1800 Hz; fstop1=600 Hz, fpass1=1400 Hz, fpass2=2200 Hz, fstop2=3000 Hz
Space filter: fspace: 1200 Hz; fstop1=0 Hz, fpass1=800 Hz, fpass2=1600 Hz, fstop2=2400 Hz

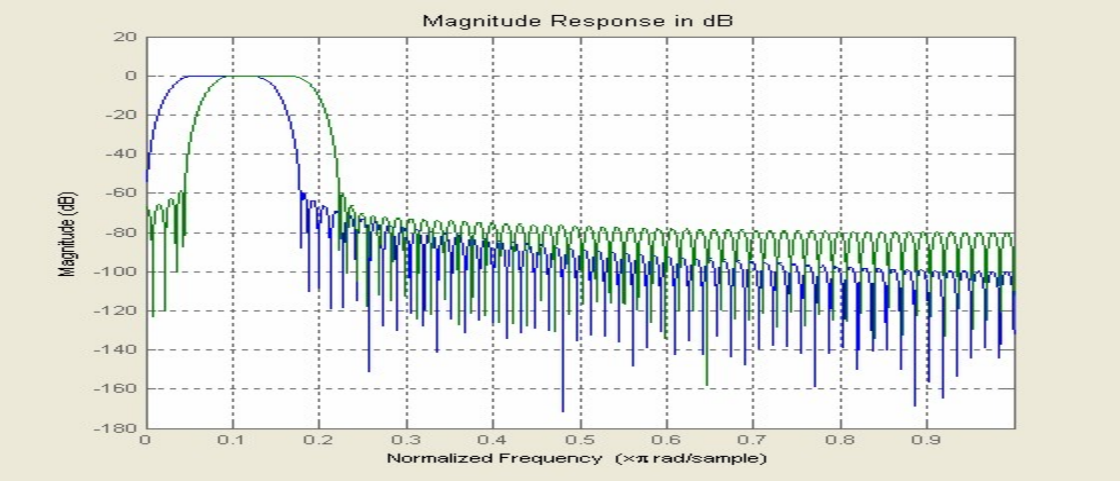

Figure 4.7: Frequency response of matched filters obtained usingwindow FIR filter design
Green: Mark filter response, Blue: Space filter response
Order: 123; Window: Kaiser (beta:0.5) fs=27 kHz, Dstop1=0.001, Dpass1=0.1, Dstop2=0.001
Mark filter: fmark: 1800 Hz; fstop1=600 Hz, fpass1=1400 Hz, fpass2=2200 Hz, fstop2=3000 Hz
Space filter: fspace: 1200 Hz; fstop1=0 Hz, fpass1=800 Hz, fpass2=1600 Hz, fstop2=2400 Hz

For example, in order to implement the sinc function shaped filters using practical filter designs, we could go for an equiripple FIR filter design or a Window type FIR filter design. The frequency response of both these types of implementations corresponding to the specifications shown above has been plotted in the figures above. As can be seen, a window type FIR filter with Kaiser window approximates the sinc function most closely, but requires a higher order/ complexity for a stable design. Even then the extent of spectral matching obtained is too poor.

Also, as the deviation frequency f_d becomes smaller compared to the sampling frequency f_s, the order of the filter increases manifold. Besides, the above designing problem, matched filter design also faces the issue of band-width. For each filter shape, there is an optimum bandwidth. In general, if the filter bandwidth is too wide, excess noise energy will be included. If the filter bandwidth is too narrow, consecutive signal elements will interfere with each other. This is called inter-symbol interference. In narrow filters, this is caused by ñringingò or by the filters inability to ñdumpò the energy of the previous element before the next element is received. Also, the assumption of white noise

interference is not justified in most real signal environments. It is also desirable that the filter perform well in non-white noise environments.

4.2 Non-coherent CPFSK demodulation techniques

The basic structure of a non-optimal CPFSK receiver, employing a non-coherent FM demodulator [23] is shown in Figure 4.8. The non-coherent demodulator requires either of the two decision methods, DM1 and DM2, explained in the following sections.

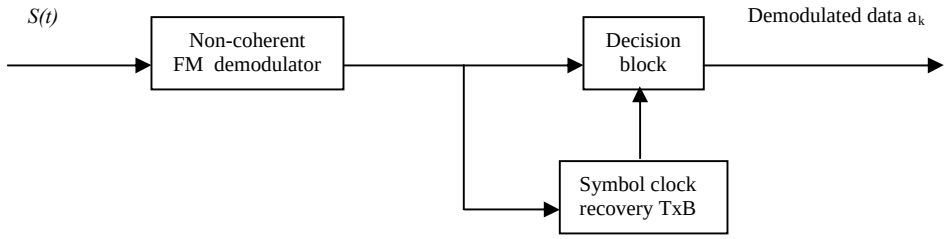

Figure 4.8: Basic structure of a CPFSK receiver, employing a non-coherent FM demodulator

4.2.1 Non-coherent FM demodulation scheme

The first stage in this class of CPFSK demodulators is non-coherent FM demodulator. Various schemes can be employed for FM demodulation at this stage. Among the various possibilities, it is found that FM discriminator based demodulator gives the best performances with decision mechanism 1 and 2.

The simplest form of frequency-modulation detector is the Slope Detector. The slope detector is essentially a tank circuit which is tuned to a frequency either slightly above or below the FM carrier frequency and has a Voltage-to-frequency response as shown in Figure 4.9(a). As the FM signal is applied to the tank circuit in Figure 4.9(b), the output amplitude of the signal varies as its frequency swings closer to, or further from, the resonant frequency of the tank. Frequency variations will still be present in this waveform, but it will also develop amplitude variations. This signal is then applied to the envelope detector in Figure 4.10(a) implemented as Figure 4.10(b), and the detected waveform is the output. This circuit has the major disadvantage that any amplitude variations in the RF waveform will pass through the tank circuit and be detected.

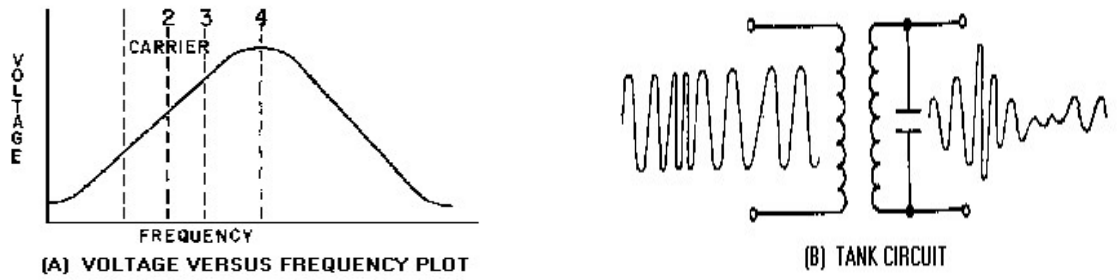

Figure 4.9: (a) Voltage vs Frequency plot of a slope detector , (b)Tank detector used in Slope detection.

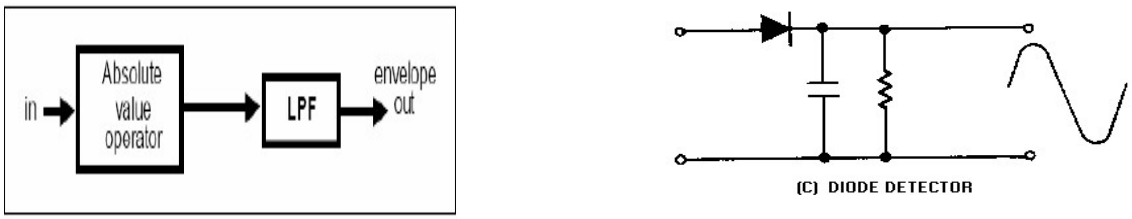

Figure 4.10: (a) Block diagram of an envelope detector (b) envelope detector.

Other possibilities include Zero- crossing detector based FM demodulation, or Foster-Seeley discriminator based FM demodulation. In our implementation, we use the following implementation of the non-coherent FM demodulator block.

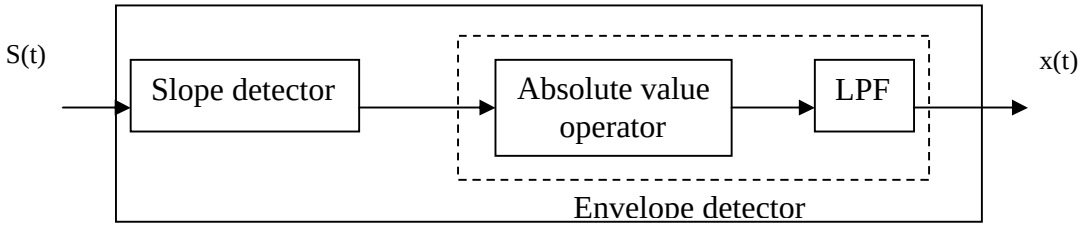

Figure 4.11: Non-coherent FM demodulator block

4.2.1.1 Implementation Issues

The slope detector is implemented using a differentiator or a high-pass filter designed using a butter-worth IIR filter. The order and other specifications of the high-pass filter used depend on the system specifications. A more efficient implementation of the slope detector is using a balanced discriminator. But in our implementation we used a differentiator. The low-pass filter used in the envelope detector is meant to remove any high frequency components, and is designed using a butter-worth IIR filter of suitable order and cut-off. In most of the low-pass butter-worth IIR filter designs, a filter order of

6 to 10 was found to serve the purpose. The cut-off specifications of-course depend on the system design.

4.2.1.2 Results and Discussions

The choice of FM demodulation technique used to obtain the base band signal, does have an impact on the BER performance at the receiver output. FM discriminator type of demodulator is known to give the best perform after zero-crossing detector based demodulator. Among FM discriminator designs, Foster-Seeley discriminator is known to give slightly better performance than slope detector based discriminators, but at the cost of increased complexity. In our simulations, we stick to slope detector based discriminators.

4.2.2 Decision Mechanism 1

Assume that x(t) is the base-band signal at the output of the FM non-coherent demodulator, expressed by (6), a_k ός are the modulating levels and *g(t)* is the pre-modulating filter impulse response.

$$x(t) = \sum_k a_k g(t - kT_s)$$

Sampling the x(t) signal at the optimum $t=kT_s$ moments would secure the correct demodulation of the modulated levels, if the impulse response of the pre-modulating filter fulfills the condition:

$$g((m-k)T_s) = \begin{cases} 1; m = k \\ 0; m \neq k \end{cases}$$

4.2.2.1 Results and Discussions

With an observation interval of 1-bit period, this decision mechanism gives a performance that is poorest of all. As the observation inter val is increased to 3- and 5- bit intervals, the performance improves and is comparable to FM-detector type FSK demodulator, but is still too inferior for most practical applications.

4.2.3 Decision Mechanism 2

By integrating the base-band signal *x(t)*, sampling the integrator output signal at the end of each symbol period and by computing the difference between two consecutive values, the phase variations $\Phi(mT_s)$, induced by the modulation over a symbol period T_s, can be obtained as shown below:

$$\int_0^{mT_s} x(t)dt - \int_0^{(m-1)T_s} x(t)dt = \int_{(m-1)T_s}^{mT_s} x(t)dt$$

$$= \frac{\phi_e(mT_s) - \phi_e((m-1)T_s)}{2 * \pi * \Delta f_{\max}}$$

$$= \Phi(mT_s)$$

When an integral response pre-modulating filter is employed, every modulating level will correspond to a certain phase variation and vice versa. Knowing the phase variation over a symbol period, the modulating level can be determined and, hence, the corresponding bits can be extracted. The advantage of this demodulation method consists in its simple implementation. The symbol clock recovery can be accomplished, employing the base-band signal x(t); as regard the integration of the x(t) signal, required for the computation of the phase variation, it can be performed by averaging the signal samples.

4.2.3.1 Results and Discussions

Figure 4.12 shows the MATLAB simulation for the performance of a defense telemetric system employing non-coherent CPFSK demodulation scheme with decision mechanism 2. The FM demodulation is performed using a Slope detector based FM discriminator.

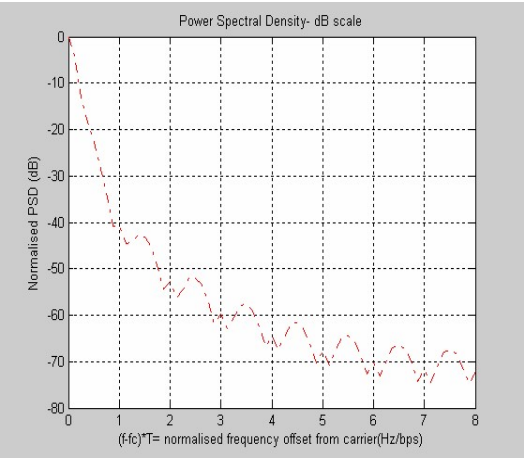

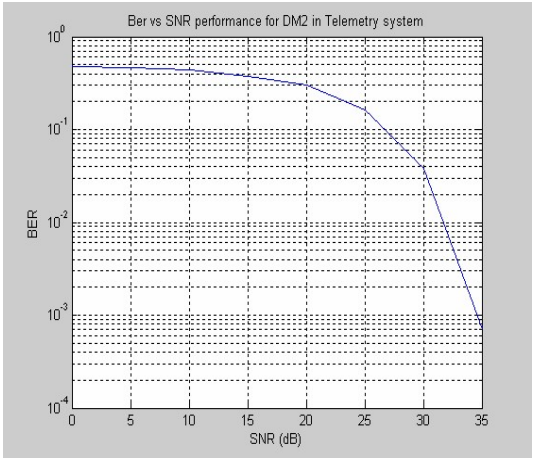

Figure 4.12: (a) PSD of the transmitted signal, (b) BER vs SNR performance. DM2
fs=9600 Hz, fc=2400 Hz, fd=30 Hz, T=32 samples, R=300bps, h=0.2, N=10000.

As can be seen from figure 4.12(a), CPFSK seems to be the right choice of modulation scheme from spectral-efficiency point of view. On the receiver side however, the choice of decision mechanism 2 does not seem to be satisfactory owing to the high BER at the SNR of practical interests. However, it was observed that the decision method 2 secured a significantly lower BER than the decision method 1on the employment of the demodulated base-band signal. So, the first decision method (DM1) is not recommendable, as long as the second one (DM2) has about the same implementation complexity.

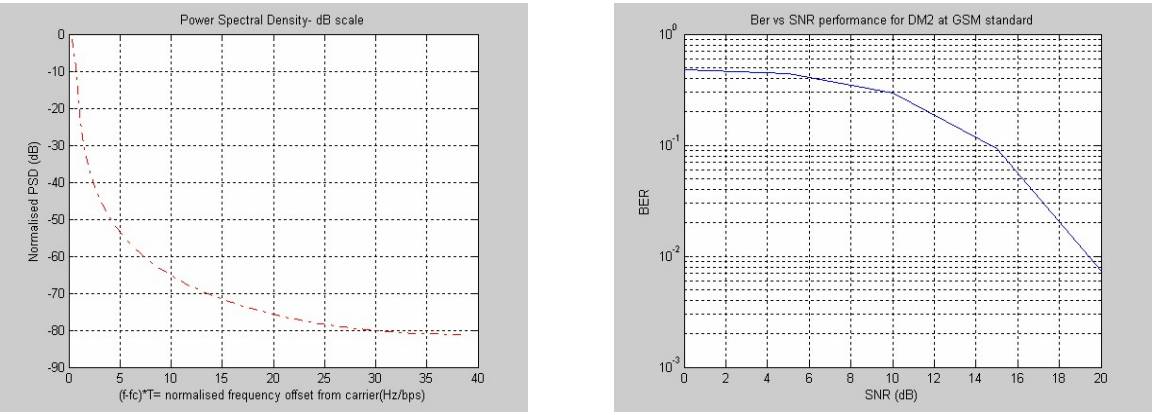

Figure 4.13: (a) PSD of the transmitted signal, (b) BER vs SNR performance. DM2
GSM standard

The same receiver was simulated at GSM standards to obtain the results shown in Figure 4.13. As can be seen, the spectral characteristics of the transmitted signal improve. Also, on the receiver side, the BER performance improves though it is still far from optimum.

From the above simulations, the BER performance of Decision Mechanism 2 was found to be influenced by the following factors:

(a) Effect of varying data-rate: Figure 4.14 shows the BER performance curves corresponding to a modulation index of h=0.5, and varying the data-rate. It is observed that the BER performance degrades as the data-rate is increased. Literature [23] suggests that the click (phase shifts of ±2´) occurrence probability increases slowly with increase in data-rate. Since, occurrence of clicks is the major source of error at low SNR, this accounts for the poor BER at low SNR, for a high data-rate scenario.

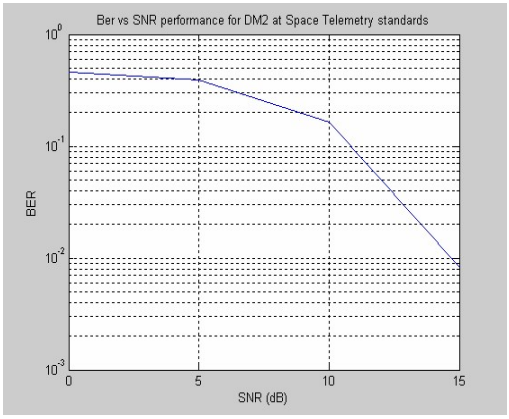

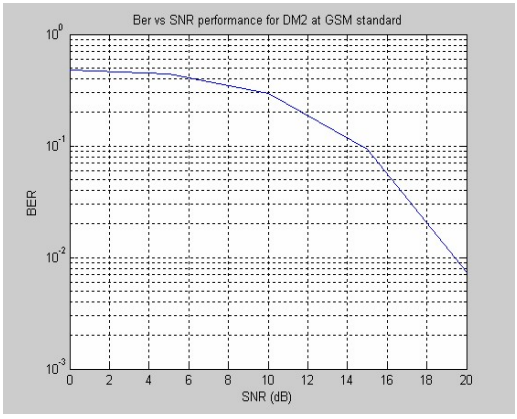

Figure 4.14: BER performance for DM 2, at h=0.5, with data-rate (a) 2400bps (b) R=280 kbps

(b) Effect of varying modulation-index: Figure 4.15 shows the BER curves corresponding to two different data-rates, with h=0.2 and h=0.5, respectively. On the basis of the previous observation, we would have expected a degradation in BER performance as the data-rate is increased. On the contrary, we observe that the BER performance improves, in spite an increase in data-rate. It can be concluded that modulation index has significant affect on BER as well. Since, h increases from 0.2 in the telemetric system to 0.5 under GSM specifications; this explains the improvement in BER performance at a given SNR. Thus, BER performance improves with increase in modulation index in (0,1), with a simultaneous increase in band-width though. Also, it can be concluded that the improvement in BER performance with increase in modulation index in (0,1) is more significant than the degradation in performance with increase in data-rate.

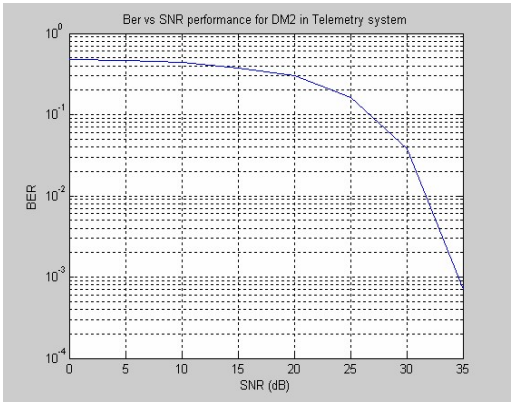

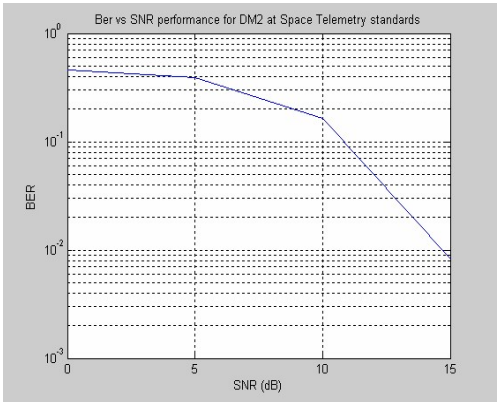

Figure 4.15: BER performance for DM-2, at (a) R=300 bps, h=0.2 (b) R=2400 bps, h=0.5

In accordance with the above facts, this receiver set-up gives satisfactory performance under following specifications.

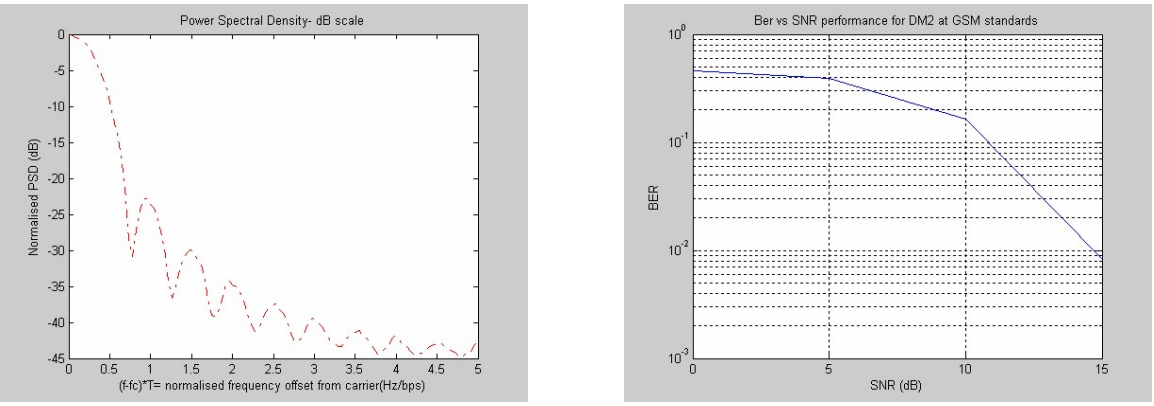

Figure 4.16: (a) PSD of the transmitted signal, (b) BER vs SNR performance DM2
(fc=1500 Hz, fd=600 Hz, h=0.5, fs=27 kHz, R=2400bps, N=10000)

4.3 Correlation filter based non-coherent demodulation technique

The receiver is implemented in three parts: a demodulator, correlation filters and a decision algorithm. The demodulator returns the real transmitted signal to a complex base band signal. Complex correlation is then done between the signal received and the two possible signals sent. The correlators output four scalar values, which are the real and imaginary parts of the received signal correlated with the possible signals sent. The decision algorithm then operates on the correlator outputs, depending on the observation interval.

Since only the real part of the complex signal has been sent, an I-Q type demodulator, shown in Figure 4.17, is used to return the received and sampled signal, r(n), to base band and obtain the real and imaginary parts of the transmitted information bearing signal.

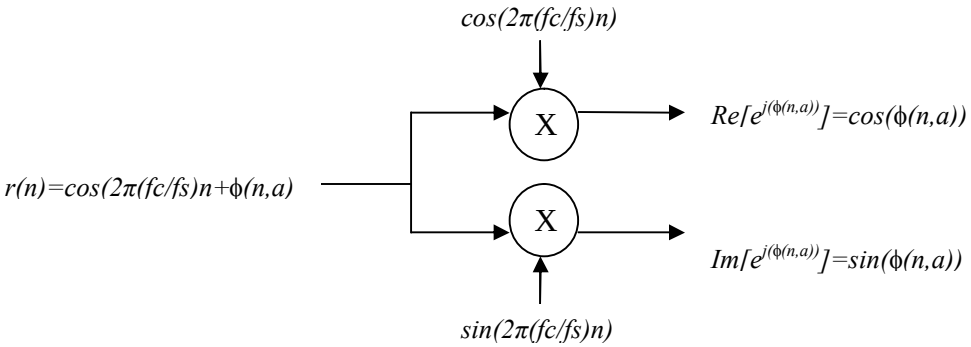

Figure 4.18: I-Q demodulator

where n = 1, 2, é , kN, with k representing the number of bits sent and N the number of samples per bit. Once the signal has been returned to base band, correlator receivers are used to determine the components of the signal sent with respect to each of the possible signals sent. From these values, a decision algorithm will make the best estimate of the data symbol sent based on a maximum likelihood block estimate [28].

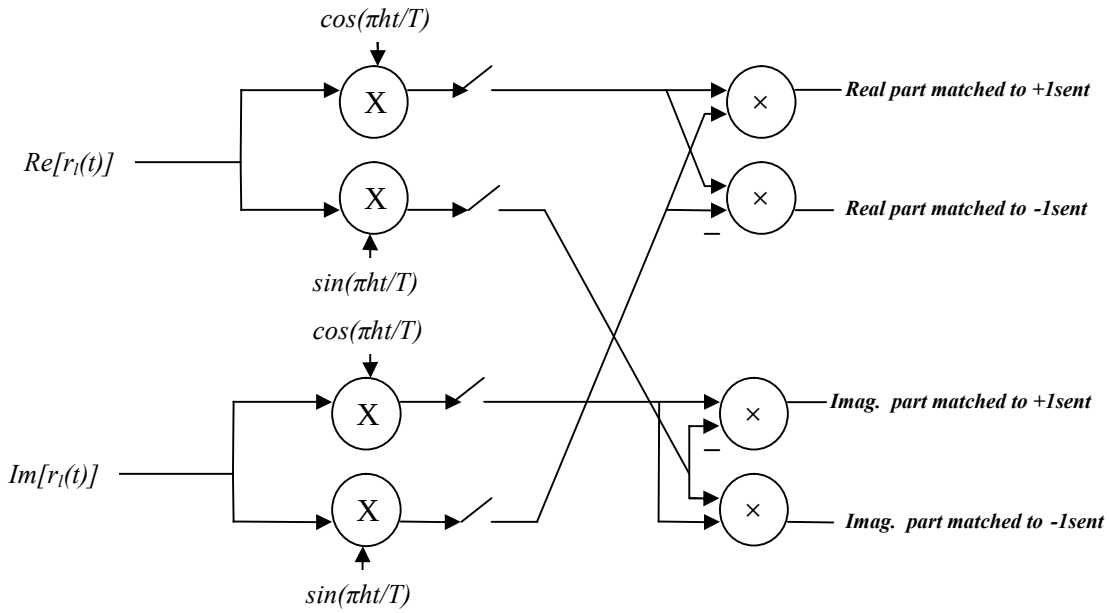

Figure 4.19: Theoretical realization of correlator receiver.

At the symbol time, T, each correlator output is integrated, sampled and recombined in such a fashion as to obtain the real and imaginary parts of the received signal correlated with each of the possible sent signals. The decision is based on the computation and comparison of certain metrics. For a one bit observation interval, it is simply the magnitude of the complex output of the correlator. The decision is made in favor of the one with larger magnitude.

For each input data vector, [28] shows that the maximum likelihood block detection metric (for binary CPFSK and a three symbol observation interval) can be written as

$$\beta_{k,l,m} = A_k + e^{-j\pi l\alpha_k}[B_l + e^{-j\pi l\alpha_l} C_m]$$

for k = 1, 2; l = 1, 2; m = 1, 2; and where A is the complex valued correlator output over the (n-2)nd bit interval, B is the complex valued correlator output over the (n-1)st bit interval and C is the complex valued correlator output over the nth bit interval. The complex constants are phase contributions from each previous symbol. Hence, (9)

calculates β for all possible data vectors. Finally, $\max[|\beta_{k,l,m}|^2]$ gives the most likely path and the middle bit is chosen accordingly. Similarly, a metric dependent on correlator output for 5-bit periods can be computed when the observation interval is 5-bit period.

4.3.1 Results and Discussions

The correlation filter type demodulator gives near optimum performance for CPFSK demodulation. Figure 4.20 illustrates the performance of CPFSK system under telemetric standards, with an observation interval of 1-bit duration. The performance is found to be satisfactory with a correlation filter based demodulator.

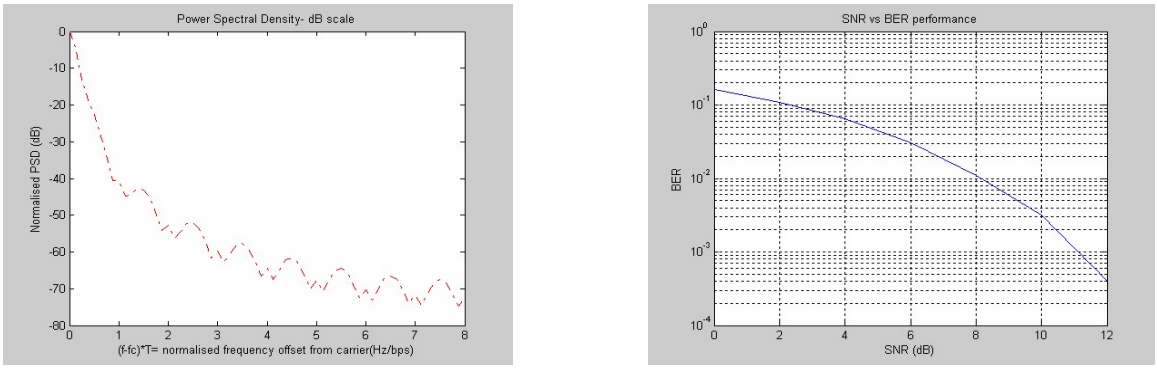

Figure 4.20: (a) PSD of the transmitted signal, (b) BER vs SNR performance. correlation receiver fs=9600 Hz, fc=2400 Hz, fd=30 Hz, T=32 samples, R=300bps, h=0.2, N=10000.

From the simulations performed, the following were observed:

(a) Effect of varying modulation index: In order to study the effect of varying modulation index on the BER performance of the receiver, the telemetric system was simulated with h=0.5 at the same data rate. The BER performance was found to be similar for SNR of practical interest as can be seen in Fig.22. From the above observations, it can be concluded that unlike a CPFSK receiver based on DM2, the performance of correlation receiver is independent of variations in modulation index h.

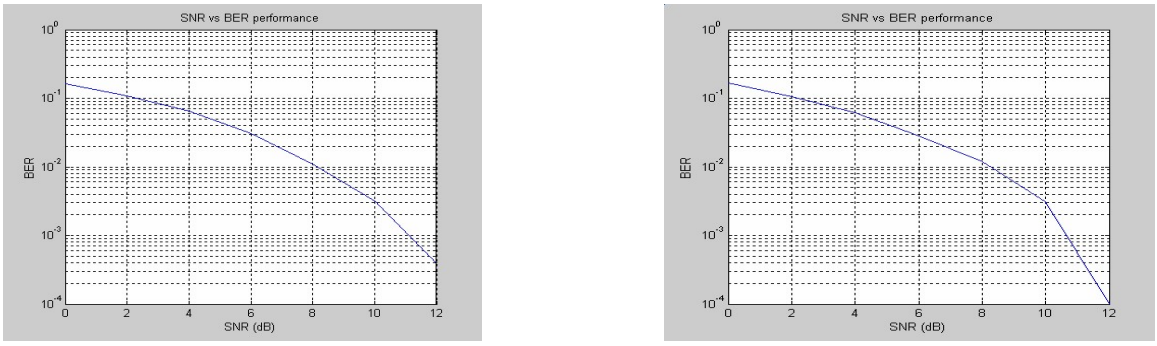

Figure 4.21: BER performance of telemetry system (a) h=0.2 (b) h=0.5. correlation receiver fs=9600 Hz, fc=2400 Hz, T=32 samples, R=300bps, N=10000.

Besides, increase in h at the same data rate resulted in a simultaneous increase in the band-width requirement.

(b) Effect of varying data-rate: In order to study the effect of varying data rate on the BER performance of the correlation receiver, the same receiver, with an observation interval of 1-bit duration, was simulated at GSM standards, and was found to give no errors for N=10000 bits. Thus, unlike the CPFSK receiver based on DM2, the performance of correlation receivers is not affected by clicks and thus, shows significant improvement with increase in data rate.

(c) Effect of varying observation-interval: In order to study the performance of the receiver with varying observation interval, the correlation receiver was simulated with observation intervals of 3- and 5-bit durations; under telemetric standards. The BER performance of the receiver, thus obtained is plotted in Figure 4.22. As is evident from the figure, the performance improves as the observation interval is increased to 3- and 5-bit durations, respectively.

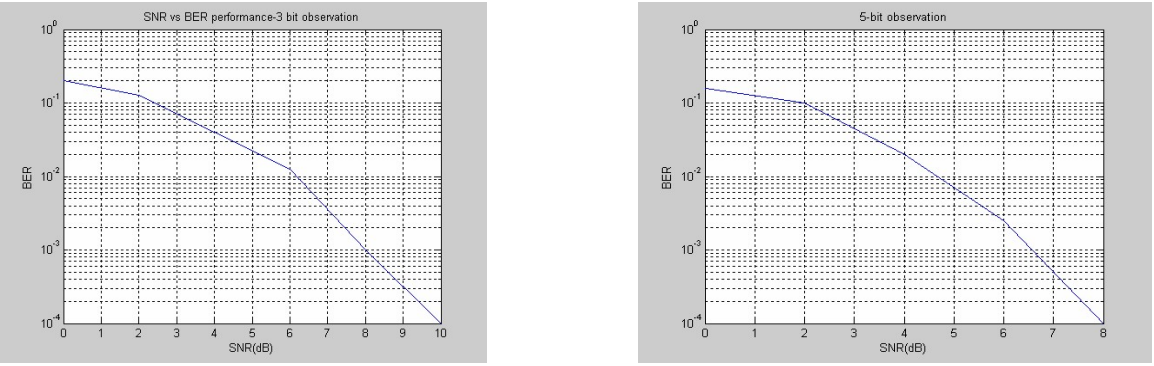

Figure 4.22: BER performance of correlation receiver with (a) 3-bit (b) 5-bit, observation interval.
fs=9600 Hz, fc=2400 Hz, T=32 samples, R=300bps, h=0.2, N=10000.

4.4 Zero- crossing based demodulation technique

The block diagram of the zero-crossing based coherent MSK demodulator is shown in Figure 4.23. The system is basically made up of a phase detector followed by a carrier and clock recovery and decision stages. The received signal $r(t) + n(t)$, after noise limiting, is fed to a zero-crossing detector (ZCD) which generates a sequence of positive

impulses at its output. In order to realize a ZCD, one would hard-limit the input waveform, differentiate to accentuate the zero-crossing points and pass through a full-wave rectifier to eliminate negative pulses due to negative-going zero crossings as shown in Figure 3.6.

The resultant signal is then low-pass filtered and integrated over a bit period to produce an output proportional to the instantaneous signal phase. Theoretically, samples of the accumulated signal phase at each zero crossing could have been obtained by directly integrating the ZCD output. However, this would enable one to know the phase values only where the zero crossings occur. As will be explained below, mid-bit and end-bit instantaneous phase values are needed for clock and carrier recovery. A low-pass filter (LPF) cascaded with the ZCD will provide the phase value at any instant over the bit period. The end-bit sample is used for the decision and the mid-bit value, together with the end-bit value, by the clock and carrier recovery stage.

Figure 4.23: ZCD based non-coherent CPFSK demodulator.

The zero-crossing block in the above figure is implemented as shown in Figure below. A coherent implementation of Figure 4.23 has already been discussed in Section 3.3. The receiver in Figure 4.23 operates non-coherently. In this case, carrier recovery is not necessary and the decision will be based on a comparison of two measured phase samples from the received signal; namely, one at the start of the bit period and the other at the end of the bit period. A decision will be made by looking at the direction of the phase change over the bit period.

The non-coherent ZCD based CPFSK demodulator can be seen as derivative of the class of CPFSK demodulators discussed in Section 4.2, where we use ZCD based non-coherent FM demodulation scheme, followed by decision method 2.

The clock recovery is achieved by a process similar to that used in the coherent implementation discussed in Section 3.3. Clock recovery is achieved by using a peak search algorithm. It uses three phase samples: two mid-bit samples from two consecutive bits and an end-bit sample between them. Considering the possibility that the phase trajectory relative to the carrier phase has a local maximum (or minimum) at the end of a bit period (this happens whenever a change in the received binary symbol occurs), the algorithm compares the differences in phase between three samples to determine the timing error.

4.4.1 Implementation issues

The issues involved in the implementation of a non-coherent ZCD based CPFSK demodulator are same as those in the implementation of a coherent ZCD based CPFSK demodulator, except that carrier and clock recover are not required in this case. Thus, all the issues discussed in section 3.3.2 hold true in this case as well. The only other difference between a coherent and non-coherent implementation becomes evident in the decision stage. Here the decision will be based on a comparison of two measured phase samples from the received signal; namely, one at the start of the bit period and the other at the end of the bit period. Thus, using the integrator output shown in Figure 4.24, corresponding to the input bit-stream shown in figure, the decision is taken as shown below.

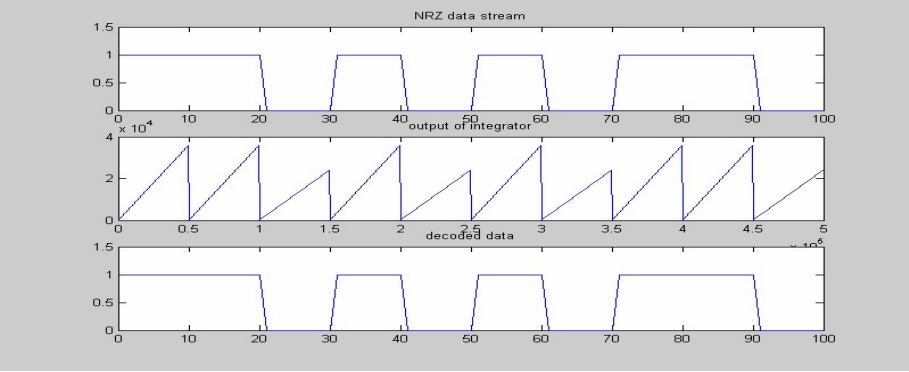

Figure 4.24: Decision making in a ZCD based demodulator, using phase information at integrator output (fc=1500 Hz, fd=600 Hz, h=0.5, fs=27 kHz, N=10)

As mentioned in section 4.4, the non-coherent ZCD based CPFSK demodulator can be seen as derivative of the class of CPFSK demodulators discussed in Section 4.2, where

we use ZCD based non-coherent FM demodulation scheme, followed by decision method 2. Every modulating level will correspond to a certain number of zero-crossings over a bit-period and vice versa. Knowing the number of zero-crossings over a symbol period, the modulating level can be determined as shown in Figure 4.24.

4.4.2 Results and Discussions

Referring to section 4.2.1.2, we know that DM2 with zero-crossing detector based FM demodulator gives the best performance. Hence, the performance of zero-crossing based demodulator is superior to FM discriminator based demodulators and comparable to correlation filter based demodulators. Figure 4.25 plots its BER performance.

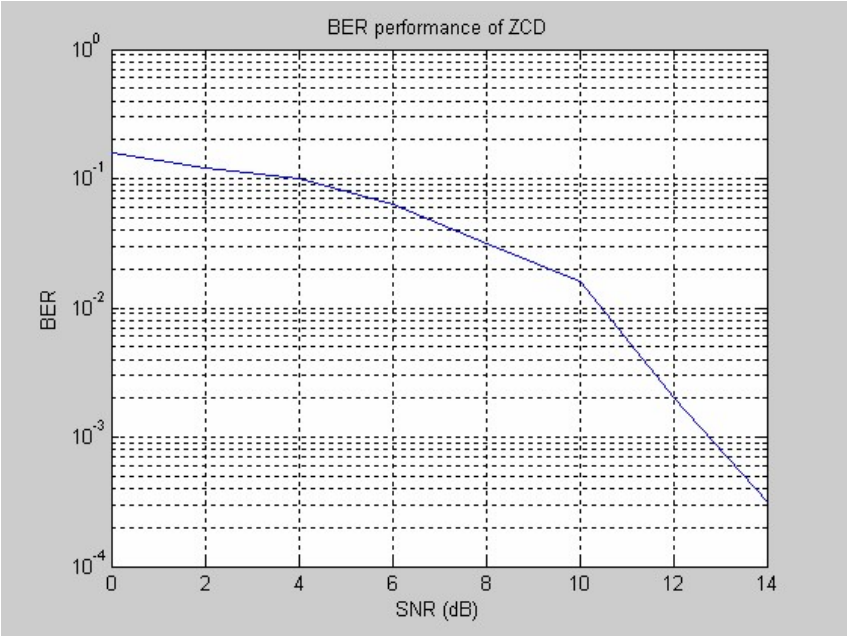

Figure 4.25: BER performance of non-coherent ZCD based receiver
fs=9600 Hz, fc=2400 Hz, T=32 samples, R=300bps, h=0.2, N=10000.

Chapter 5
Summary

5.1 Summary

In this thesis, we analyzed various CPFSK demodulation schemes and compared there performance with respect to BER and implementation complexity. In Chapter 2, schemes for performing CPFSK demodulation were discussed. We then analyzed the spectral characteristics of the CPFSK signal. In Chapter 3, coherent demodulation schemes for CPFSK were discussed.

In Chapter 4, various non-coherent demodulation schemes were investigated for the demodulation of CPFSK signals. It was observed that though non-optimal, this class of methods is far simpler to implement than the conventional and optimal coherent demodulation combined with Viterbi Algorithm. Besides, depending on the system specifications such as band-width, power, and required BER performance, a judicious selection from amongst the given schemes can be made to give the desired outcome, at a reduced complexity. The non-coherent CPFSK demodulation scheme discussed in section 4.2 gives satisfactory performance at defense telemetry standards and can be used for the same. Correlation filter based non-coherent demodulation scheme gives satisfactory performance at GSM standards in an AWGN channel, and at most of the telemetry standards. ZCD based non-coherent demodulation scheme gives satisfactory performance at space telemetry standards and can be used for the same.

5.2 Possible Future Extensions

The possible scope of future extension in this field lies in the area of developing and investigating non-coherent demodulation schemes for CPFSK signals with partial response pre-modulating filters, as our work has been primarily focused on integral response signals. Such systems will need to devise more robust techniques to mitigate the effect of inter-symbol interference.

Another interesting area for future extension lies in the field of adaptive CPFSK signaling. Designing non-coherent demodulation schemes that would adaptively modify themselves with varying modulation index, must be really challenging. The issues involved in this might be such as: detection of change in modulation index, adaptive filter design, adaptive thresholding in decision block, and if need be, switching from one demodulation scheme to another demodulation scheme, that gives improved performance at modified specifications.

REFERENCE

[1] Fonseka, J. P.: 'Nonlinear continuous phase frequency shift keying', *IEEE Trans.,* 1991. COM-39, pp. 1473-1481.

[2] M. G. Pelchat, ñThe autocorrelation function and power spectrum of PCM/FM with random binary modulating waveforms,ò *IEEE Trans. Space Electron. Telem.,* pp. 39-44, Mar. 1964.

[3] Aulin, T., and Sundberg, C.W., ñCPM-An Efficient Constant Amplitude Modulation Scheme,ò *Int. J. Satellite Commun.,* vol. 2, pp. 161-186, September, 1982.

[4] Aulin, T., and Sundberg, C.W., ñMinimum Euclidean Distance and Power Spectrum for a Class of Smoothed Phase Modulation Codes with Constant Envelope,ò *IEEE Trans. Commun.,* vol. COM-30, pp. 1721-1729, July, 1982.

[5] G . D. Forney, Jr., ôThe Viterbi algorithm,ò *Proc. IEEE, vol. 61, pp. 268-278, Mar. 1973.*

[6] S. Pasupathy, ñMinimum Shift Keying: A spectrally efficient modulation", *IEEE Communications Magazine*, Vol. 17, pp. 14 -22, 1979.

[7] K. Feher, ñModems for emerging digital cellular mobile radio systems", *IEEE Transactions on VehicularTechnology*, Vol. VT-40, pp. 355-365, 1991.

[8] Y.L. Huang, K.D. Fan and C.C. Huang,ñA fully digital non-coherent and coherent GMSK receiver architecture with joint symbol timing error and frequency offset estimation", *IEEE Transactions on Vehicular Technology*, Vol. VT-49, pp. 863 - 873, 2000.

[9] R. Prasad, W. Mohr and W. Konhauser, *Third Generation Mobile Communication Systems*, Boston, Artech House, 2000.

[10] T. Rappaport, *Wireless Communications: Principles and Practice,* New Jersey Prentice Hall, 2002.

[11] Y. Li, S. M. Goldwasser, M. Bystrom, P. Herczfeld, ñGeneration of MSK Modulated Millimeter wave Sub-carrier for Radio Over Fiber Applications,ò Drexel University, Philadelphia, 2003.

[12] W. Zhuang, W. A. Krzymien, P. A. Goud, ñTrellis-coded CPFSK and soft-decision feedback equalization for micro-cellular wireless applications,ò *Springer Netherlands, Engineering*, vol.1, no. 4, Dec 1994.

[13] Sookwan Kim, Namjung Cho and Yong-Hwan Lee, ñAdaptive CPFSK Modulation for Power Line Communications,ò *IEEE Trans. Commun.*, vol.45, pp.1218-1230, Oct. 1997.

[14] Ara, S. and Horan, S. B., ñDevelopment of a New Modulation Standard for Telemetry Systems,ò *NMSU Klipsch School of Electrical and Computer Engineering Technical Report Series, Dec.1996.*

[15] Anderson J., Aulin T., and Sundberg C.-E., *Digital Phase Modulation*, Plenum Press, New York, 1986.

[16] Aulin, T., Rydbeck, N., and Sundberg, C.W., ñContinuous Phase Modulation -Part II: Partial Response Signaling,ò *IEEE Trans. Commun.*, vol. COM-29, pp. 210-225, March, 1981.

[17] Aulin, T., and Sundberg, C.W., ñContinuous Phase Modulation-Part I: Full Response Signaling,ò *IEEE Trans. Commun.*, vol. COM-29, pp. 196-209, March, 1981.

[18] Aulin, T., and Sundberg, C.W., ñOn the Minimum E uclidean Distance for a Class of Signal Space Codes,ò *IEEE Trans. Inform. Theory*, vol. IT-28, pp. 43-55, January, 1982.

[19] M. G. Pelchat, R**.** C. Davis, and M. B. Luntz, ñCoherent demodulation of continuous phase binary FSK signals,ò in *Proc. Int. Telemetry Conf.,* Washington, D. C., 1971.

[20] DeBuda, ñCoherent demodulation on frequency-shift keying with low deviation ratio,ò *IEEE Trans. Commun.* (Concise Paper), vol. COM-20**,** pp. 429-435**,** June 1972**.**

[21] G. Pelchat and S. L. Adams, ñNon-coherent detection of continuous phase binary FSK,ò in *Proc. Int. Conf. Communications.* Montreal. P.Q.Canada , 1971.

[22] W.P. Osborn and M.B. Luntz, ñCoherent and noncoherent detection of CPFSK", *IEEE Trans. on Communications*, Vol. COM-22, pp. 1023-1036, 1974.

[23] Zsolt, A.,and Polgar, Vasile Bota, ñSimplified Demodulation Methods of CPFSK Signals Performances and Digital Implementation Aspects,ò PhD thesis, Communications Dept., Technical Univ. Romania, 2003.

[24] Eric S. Otto, and Philip L. De Leon, ñDigital CPFSK Transmitter and Non-coherent Receiver/ Demodulator Implementation,ò *NMSU Center for Space Telemetry and Telecommunications Technical Report Series, Dec.1996.*

[25] Mine Kalkan, and Feza Kerestecio Glu, ñZero-Crossing Based Demodulation of Minimum Shift Keying,ò *Turk J Elec Engin*, vol.11, no.2, 2003.

[26] Bob Watson, ñFSK: Signals and Demodulation,ò *WJ Tech-note*, Vol.7, no. 5, September/October, 1980. Reprinted in 2001.

[27] Karim Hamidian, ñClosed Form of the Power spectral density of M-ary CPFSK Modulation,ò *Computers Elect. Engg* Vol. 20, No. 3, pp. 259-271, 1994.

[28] Simon, M.K. and Divsilar, D., ñMaximum-likelihood Block Detection of Non-coherent Continuous Phase Modulation,ò *IEEE Transactions on Communications*, Jan. 1993.